# *A combined photoionization time-of-flight mass spectrometry and laser absorption spectrometry flash photolysis apparatus for simultaneous determination of reaction rates and product branching*



**As Published:** 10.1063/1.5024399

**Publisher:** AIP Publishing

**Persistent URL:** https://hdl.handle.net/1721.1/135828

**Version:** Final published version: final published article, as it appeared in a journal, conference proceedings, or other formally published context

# A combined photoionization time-of-flight mass spectrometry and laser absorption spectrometry flash photolysis apparatus for simultaneous determination of reaction rates and product branching

Joshua E. Middaugh,[1,a)] Zachary J. Buras,[1] Mickael Matrat,[1,2] Te-Chun Chu,[1] Young-Seok Kim,[1,b)] Ionut M. Alecu,[1,c)] AnGayle K. Vasiliou,[1,d)] C. Franklin Goldsmith,[1,e)] and William H. Green[1,f)]

[1]*Department of Chemical Engineering, Massachusetts Institute of Technology, Cambridge, Massachusetts 02139, USA*

[2]*Department of Chemical Engineering, UCP, ENSTA ParisTech, Universite Paris-Saclay, 91762 Palaiseau Cedex, France*

(Received 31 January 2018; accepted 4 July 2018; published online 23 July 2018)

In recent years, predictions of product branching for reactions of consequence to both combustion and atmospheric chemistry have outpaced validating experiments. An apparatus is described that aims to fill this void by combining several well-known experimental techniques into one: flash photolysis for radical generation, multiple-pass laser absorption spectrometry (LAS) for overall kinetics measurements, and time-resolved photoionization time-of-flight mass spectrometry (PI TOF-MS) for product branching quantification. The sensitivity of both the LAS and PI TOF-MS detection techniques is shown to be suitable for experiments with initial photolytically generated radical concentrations of $\sim 1 \times 10^{12}$ molecules cm$^{-3}$. As it is fast ($\mu$s time resolution) and non-intrusive, LAS is preferred for accurate kinetics (time-dependence) measurements. By contrast, PI TOF-MS is preferred for product quantification because it provides a near-complete picture of the reactor composition in a single mass spectrum. The value of simultaneous LAS and PI TOF-MS detection is demonstrated for the chemically interesting phenyl radical + propene system. *Published by AIP Publishing.*
https://doi.org/10.1063/1.5024399

## I. INTRODUCTION

Over the past 100 years, there have been many experiments directly probing radical decay kinetics, often with the aid of lasers, and in more recent decades, there have been many predictions of the product branching of such reactions using quantum chemistry combined with rate theory. However, there have been a few experiments that directly quantify product branching against which to validate predictions. Even for a system like hydroxyl radical (OH) + acetylene ($C_2H_2$) that is critical for both combustion and atmospheric chemistry, there is limited experimental validation of the predicted branching,[39] which has subsequently been incorporated into many common combustion mechanisms.[43]

The few experiments that do attempt to quantify product branching usually fall into three categories: crossed molecular beams (CMBs) that simulate a single-collision environment,[18] end-product analysis of a complex process such as pyrolysis, or flash photolysis coupled to a fast detection technique. In the case of CMB experiments, although the dynamics and energetics of a specific reaction can be probed with exquisite detail, it is difficult to connect these results to the thermalized environment of many applications. In the case of end-product analysis, a detailed chemistry mechanism with many parameters is often needed to interpret the results, which leads to large uncertainty in the final product quantification. Some successful examples of quantitative end-product analysis are flow pyrolysis reactors combined with gas chromatography/mass spectrometry (GC/MS)[44] and flash pyrolysis reactors combined with both molecular beam MS (MBMS)[64] and infrared spectroscopy.[5] Flash photolysis offers a compromise between these two extremes: the reaction environment is thermalized, but the chemistry is simple enough that secondary and side reactions can often be neglected. Time-resolved detection techniques such as absorbance,[28] laser induced fluorescence (LIF),[45] and MBMS[2] are frequently used with flash photolysis to obtain product branching. Combining two of these techniques, absorbance and MBMS, in one flash photolysis reactor allows for complementary measurements of both overall kinetics and product branching with high-fidelity.

In order to directly measure the chemical kinetics of specific reactions, it is necessary to probe the concentration of either one of the reactants or one of the products with a time-resolution sufficient to resolve the transient decay or rise of the probed reactant or product, respectively. To accomplish this task, both time-resolved MBMS and laser absorption spectrometry (LAS) can be used. However, LAS is traditionally

a)Present address: Air Products and Chemicals, Inc., Allentown, Pennsylvania 18195, USA.
b)Present address: The Dow Chemical Company, Marlborough, Massachusetts 01752, USA.
c)Present address: Alecu Radiation Oncology Services (AROS, LLC), Colleyville, Texas 76034, USA.
d)Present address: Department of Chemistry and Biochemistry, Middlebury College, Middlebury, Vermont 05753, USA.
e)Present address: School of Engineering, Brown University, Providence, Rhode Island 02912, USA.
f)Author to whom correspondence should be addressed: whgreen@mit.edu

better suited for kinetic measurements because it is fast and non-intrusive, and one can usually design the initial mixture so its absorption spectrum does not block the expected transient absorption of the radicals.

In order to measure the product branching fractions of a chemical reaction, it is necessary to quantitatively determine the amount of each product species relative to the total concentration of the limiting reactant or to all other products. Single-wavelength LAS is not convenient for measuring branching ratios because usually one would need to do experiments at more than one probe wavelength and also one would need absolute calibrations of the absorption cross sections of each species at each probe wavelength at all temperatures ($T$) and pressures ($P$) considered. While it is possible to measure product fractions using LAS,[28] in most cases, mass spectrometry is generally more suited for product quantification as it can in principle determine the difference in abundance of any species with different masses. Therefore, in order to measure both chemical kinetics of reactions with high resolution and product branching fractions of chemical reactions, we have designed and built a novel apparatus that is the first to combine the LAS technique and the time-resolved TOF-MS technique in a single device.

Laser absorption spectrometry is a technique wherein the concentration of a species is determined by measuring the fraction of light that is absorbed. The concentration is given by the Beer-Lambert law, which says the absorbance ($A$), defined as the natural logarithm of the ratio of the initial intensity of light ($I_0$) to the final intensity of light ($I$), is proportional to the concentration of the absorbing species ($C$), the path length for absorption ($l$), and the absorption cross section of the species ($\sigma$). By measuring the transient absorbance from a single species, one can then determine its relative transient concentration. If the cross section at the wavelength of light being used and the absorption path length are known, then one can determine the absolute concentration of the species,

$$A = \ln\left(\frac{I_0}{I}\right) = \sigma l C. \quad (1)$$

The LAS technique has been used by a number of groups to determine the kinetics of various chemical reactions. In particular, the group in the Combustion Research Facility at Sandia National Laboratory has used a multiple-pass absorption cell for studying gas-phase chemical kinetics.[38] This multiple-pass design was the inspiration for an earlier apparatus built in our group.[22–24] The laser systems (both the photolysis laser and the composite Ti:Sapphire laser system), the basic design for the multiple-pass absorption configuration, the optical layout (including the beam shaping optics for the Ti:Sapphire laser and the telescoping optics for the photolysis beam), and the differential amplification and signal detection scheme used in Ismail *et al.*'s apparatus are also used in the new apparatus. Some changes and improvements were made to these systems to accommodate the new instrument, which are discussed later in this work.

Compared to pump-probe techniques such as laser induced fluorescence (LIF), LAS is much less sensitive to pulse-to-pulse fluctuations in the photolysis shot because a complete time trace is recorded for every shot. However, single-pass LAS is usually not sufficient to detect the low radical concentrations ($\sim 10^{12}$ cm$^{-3}$) necessary to avoid excessive radical-radical reactions. Therefore, multiple-pass LAS is usually necessary and the Herriott cell design used here is preferable to other multiple-pass configurations, such as a White cell,[58] due to its relative simplicity (only two mirrors), stability, and control over the probed volume.

Time-resolved Photoionization Mass Spectrometry (PIMS) is a technique wherein a sample of a reactive mixture is ionized using light, usually in the vacuum ultraviolet (VUV) range, and then analyzed with enough time resolution to ascertain the time-dependence of the relative abundance of the ions separated by their mass-to-charge (m/z) ratios. Provided that the photoionization process is mostly single-photon (i.e., only one photon of ionizing radiation is absorbed per molecule), then the charge imparted to each ionized molecule is +1, and the only difference between the ions is their mass. Thus by applying a static electric field in the case of time-of-flight mass spectrometry or an oscillating radio-frequency field in the case of quadruple mass spectrometry, the ions can be separated according to their masses with the abundance of each mass being proportional to the integrated signal for each mass-to-charge peak. The general time-resolved PIMS technique has been famously used by a number of groups to study the kinetics and the time-dependent species distribution of chemical reactions. Instruments include those from Fockenberg *et al.*,[16] Slagle and Gutman,[41,42] Eskola and Timonen,[13,14] Blitz *et al.*,[4] and Osborn *et al.*[36]

The real challenge of *time-resolved* PIMS, and thus the reason the number of research groups using it is limited to date, is to sample the reactive mixture without altering its composition in any way. For example, the reactive mixture cannot merely be sampled by a tube fed into a generic bench-top mass spectrometer since the mixture would continue to react while in transit to the mass spectrometer and/or the reactive intermediates would be quenched by the metal walls of the tubing, thus changing the composition of the sample when it reaches the mass analyzer. More advanced techniques are required to sample the gas and maintain its composition by quickly transporting it to the mass spectrometer for analysis before it can react further with itself or with other spurious entities. Typically, such techniques involve using a custom-built apparatus to closely couple the reaction cell and the mass spectrometer together. Furthermore, all of the aforementioned designs including our design utilize an effusive or a supersonic expansion to sample the reactive gas. Such an expansion of the gas sample accomplishes several desired objectives at once. First, it attenuates the gas and drops the pressure by several orders of magnitude to approach the high-vacuum (low-pressure) environment required to use a mass spectrometer. Typically, a second stage of pumping with a conical skimmer is used to further attenuate the gas and thus reduce the pressure even further, with the exception being the design of Blitz *et al.*[4] where the snout of the TOF-MS is coupled directly to the effusive expansion. Second, the gas expansion cools the reactive mixture and maintains the composition of the gas sample during transit to the mass spectrometer. Finally, the collisions in the gas sample during the finite transit time to the PIMS are greatly reduced as a result of the attenuated gas density and as a result

of the greatly accelerated motion in the direction away from the pinhole toward the PIMS. Therefore, the molecules in the gas sample quickly reach the ionization region of the mass spectrometer (typically in 10–100 $\mu$s) before bimolecular reactions can occur to any measurable extent.

The existing time-resolved PIMS designs do have some rather substantial differences however. For example, the designs use different methods for photoionization. Slagle and Gutman,[41,42] Fockenberg *et al.*,[16] and Eskola and Timonen[13,14] use the VUV emission from lamps to photoionize the gas sample. Blitz *et al.*[4] also included the capability to use lamps in their design but found better performance using the frequency-tripled 355 nm output of an Nd:YAG laser to obtain 118.2 nm light. Both Osborn *et al.*[36] and Sztáray *et al.*[47] use tunable VUV radiation from a synchrotron. The essentially continuous source of narrow-bandwidth tunable VUV light (7.2-25 eV with a 2.5% bandwidth) from the synchrotron is by far the best photoionization source in existence, as it allows species with different ionization energies to be analyzed and it even allows some isomers of the same m/z to be separated based on differences in their photoionization efficiency curves (i.e., isomers of the same m/z can be differentiated by observing the change in signal with respect to photoionization energy).[10] The photoionization energy range available with lamps is quite limited, and it is plagued by large gaps in the available range, relatively low photon fluxes, and multiple output photon energies.[26] The higher-order harmonics of lasers offer both very narrow bandwidths and the largest number of photons per shot (and thus the highest number of ions per mass spectrum). Compared to a synchrotron source where a continuous beam of $\sim 1 \times 10^{13}$ photons/s is generated, a pulsed VUV laser generates $\sim 1 \times 10^{11}$ photons in 5-10 ns. For kinetically relevant time scales of ~100 $\mu$s, a synchrotron will only output $1 \times 10^{9}$ photons, necessitating significant signal averaging to achieve signal to noise, S/N, levels comparable to the pulsed laser ionization source. However, the pulsed nature of lasers combined with their limited repetition rates means that the time-dependence of the mass spectra cannot be observed for each photolysis shot. Instead, it must be obtained by sequentially measuring a mass spectrum for each desired time during the course of the reaction from separate photolysis shots. That is, time resolution is accomplished by delaying the photoionization pulse relative to the photolysis pulse to obtain mass spectra at different reaction times. Lasers are also difficult to tune in the VUV range, requiring a complex setup to accomplish a narrow tuning range of even a few eV.[35]

Another difference between the existing PIMS devices is in the type of mass spectrometer used. In particular, the oldest design by Slagle and Gutman uses a quadrupole mass spectrometer (Q-MS) instead of a TOF-MS. This offers several advantages and several disadvantages. An advantage is that a single m/z peak can be monitored very rapidly by a Q-MS when a continuous photoionization source is utilized.

TABLE I. Comparison of time-resolved PIMS devices in the literature.

| Publication | Reactor | Pinhole φ (mm) | *T* range (K) | *P* range (Torr) | PI source | MS |
|---|---|---|---|---|---|---|
| Slagle and Gutman[42] | 51 cm long<br>1.05 cm ID<br>Quartz | 0.44 | 300–811 | 1 | ARL[a] | Q-MS[b] |
| Fockenberg *et al.*[16] | 43 cm long<br>1.0 cm ID<br>Quartz | 1.0 | 300–873 | 10 | ARL[a] | TOF-MS[c] |
| Eskola and Timonen[13] | 43 cm long<br>0.6/0.8/1.7 cm ID<br>Coated stainless steel | 0.15/0.3/0.5 | 200–360 | 0.2–40 | ARL[a] | Q-MS[b] |
| Blitz *et al.*[4] | 70 cm long<br>1.3 cm ID<br>Quartz | 1.0 | 300–1000 | 0.5–2 | Ninth Nd:YAG[d] or ARL[a] | TOF-MS[c] |
| Osborn *et al.*[36] | 62 cm long<br>1.05 cm ID<br>Quartz | 0.4/0.65 | 300–1050 | 1–10 | Tunable synchrotron | TOF-MS[c] |
| Sztáray *et al.*[47] | 60 cm long<br>1.05 cm ID<br>HW[f]-coated quartz | 0.3 | 300 | 1–4 | Tunable synchrotron | PEPICO[e] |
| This work | 100 cm long<br>1.6/3.6 "bow-tie" ID<br>Quartz | 0.3 | 300–800 | 1–50 | Ninth Nd:YAG[d] | TOF-MS[c] |

[a]ARL = Atomic Resonance Lamp.
[b]Q-MS = Quadrupole MS.
[c]TOF-MS = Time-of-Flight MS.
[d]Ninth Nd:YAG refers to the ninth harmonic wavelength of an Nd:YAG laser (118 nm, 10.5 eV).
[e]PEPICO = Photoelectron Photoion Coincidence spectroscopy.
[f]HW = Halocarbon Wax.

This allows the kinetics of a single m/z peak to be observed for every photolysis shot with both high time resolution and signal to noise level(s). However, a Q-MS cannot scan the mass range quickly enough to observe more than one m/z peak at a time, as the mass-scanning time is longer than the typical reaction time scales. Therefore, the time dependence of each mass peak in Q-MS must be recorded individually, meaning that a Q-MS is not multiplexed like TOF-MS wherein the entire mass spectrum is recorded at once. For TOF-MS with a pulsed ionization source, measurements of relative product branching are less sensitive to drifts and fluctuations in photolysis laser and VUV intensity than they would be for Q-MS, as the relative abundance of each m/z peak is recorded for each photolysis/VUV shot. Thus, for the same total acquisition time, the trade-off between using a continuous Q-MS versus a TOF-MS is to have more precise kinetic measurements *in lieu* of more precise relative mass abundances, which are required to obtain more precise product distributions. If an experiment were to use a Q-MS with a pulsed ionization source, instead of the traditional pairing with a continuous ionization source, then the Q-MS would have clear disadvantages, having neither the advantage of the fast detection of a Q-MS with a continuous ionization source nor the advantage of the multiplexed detection of a TOF-MS. Most of the more recent PIMS instruments use TOF-MS to take advantage of its multiplexed nature and to exploit its ability to more precisely determine product distributions. A summary of the similarities and differences between the known time-resolved PIMS devices is shown in Table I.

While we mostly took inspiration for the design of the PI TOF-MS portion of the new apparatus from the designs by Osborn *et al.* and by Blitz *et al.*, the additional incorporation of multiple-pass LAS is a new feature that required some unique reactor and chamber design. Specifically, the reaction cell dimensions have to be large enough to accommodate the passage of the multiple-pass laser beam while still ensuring that the TOF-MS is sampling from a fully illuminated (i.e., narrow diameter) section of the reactor. Additionally, the custom vacuum chamber had to allow close coupling of the PI TOF-MS to the reaction cell and thus to the multiple-pass LAS.

## II. EXPERIMENT

### A. Reaction cell

Figures 1–3 show the apparatus from different angles and cross-sectional views. The apparatus consists of a "bow-tie-shaped" custom quartz flow reactor housed in a custom vacuum chamber. The reactor is 1 m long in total and has a 1.6 cm ID (2.5 mm wall thickness) in its central 40 cm and a 3.6 cm ID (2.0 mm wall thickness) everywhere else. The narrow ID at the center of the reactor is matched by the diameter of the photolysis laser (described in Sec. II B) used to generate radicals. As a result, radial diffusion of photolytically generated radicals and subsequent products is eliminated as a loss process in the center of the reactor where sampling for TOF-MS occurs. The larger diameter at the edges of the reactor is necessary to accommodate the Herriott cell.

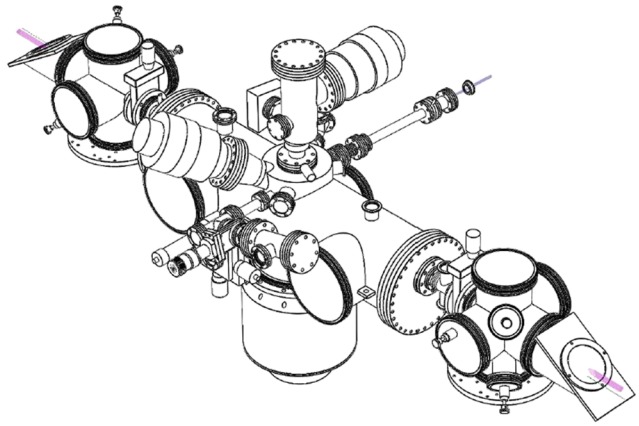

FIG. 1. Isometric view of the LAS/PI TOF-MS chamber. Photolysis beam is shown in pink, probe beam is shown in green, and photoionization beam is shown in blue.

To prepare the reactive gas mixture, a manifold of calibrated mass flow controllers is used to flow precisely controlled amounts of each component. The gas mixture flows in through the tube on the left of the chamber and out through the port on the right of the chamber. Although not shown in the diagram, the exit port is connected to an automated butterfly valve to actively control the pressure in the reaction cell between 1 and 1000 Torr using a feedback controller. The outlet of the automated pressure control valve is connected to a Leybold WSU251/D65BS Roots blower pump package via a long 3″ diameter stainless steel tube that runs from the laboratory to a separate pump room. This Roots blower has a pumping speed of about 300 $m^3$/h (~$10^6$ SCCM), which is more than sufficient to handle the 1000 SCCM maximum flow for a typical experiment and still keep the pressure at the inlet to the Roots blower in the 100s of millitorr range. At all reactor temperatures and pressures, the total gas flow rate was chosen such that the residence time from the reactor inlet to outlet was 1 s: ~$10^{-3}$ $m^3$/s volumetric flow rate or ~2 m/s linear velocity. Using this relatively low flow rate has several advantages. First, pressure drop across the reactor is negligible (~0.01 Torr) as verified by measuring the pressure upstream of the reactor. Second, it was possible to achieve the relatively flat temperature profiles shown in Fig. 4. Finally, at these conditions, there is an ~50 ms window of time after photolysis during which time-resolved MS can be measured free of convective transport effects.

The reactor is heated by Nichrome ribbon wire in two zones. First, there is a 5 cm pre-heat zone slightly upstream of where the Herriott cell and photolysis laser overlap (see Sec. II B, referred to as the Herriott cell overlap region) that rapidly brings the room temperature flowing gas mixture to the desired temperature. Then there is a reaction zone that maintains the gas at near isothermal conditions for almost the entire remaining length of the reactor (up to the last 20 cm). The temperature of the gas leaving each zone is measured by a thermocouple inside the reactor and out of the path of the photolysis laser and Herriott cell. The thermocouple reading is used to control the power provided to each heated zone. Using this scheme, the temperature in the central 0.5-0.6 m corresponding to the overlap region only varies up to ±3%

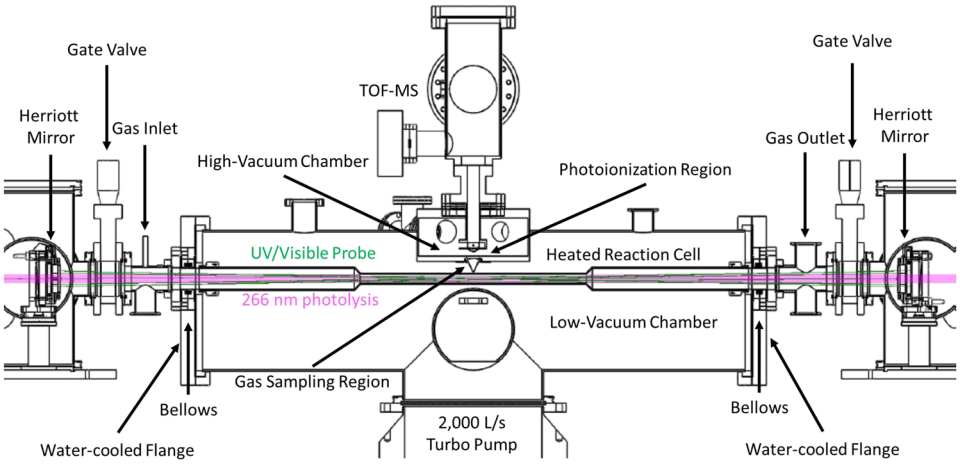


FIG. 2. Front cross sectional view of the LAS/PI TOF-MS apparatus showing the reaction cell as well as the gas sampling region in the center.

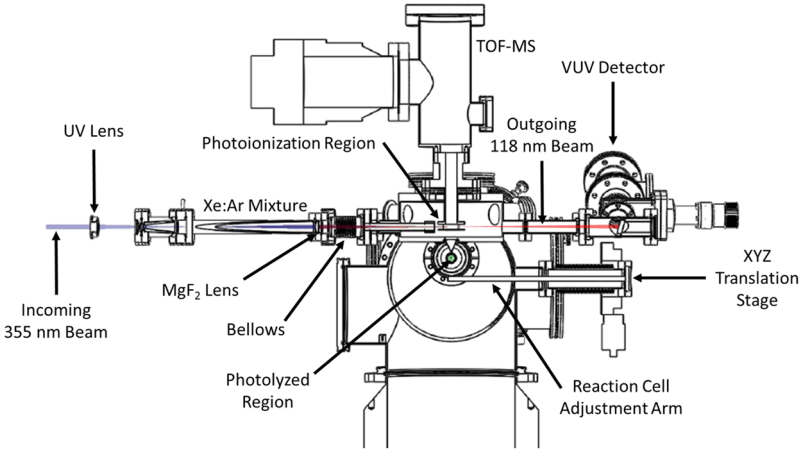


FIG. 3. Side cross sectional view of the LAS/PI TOF-MS apparatus showing the VUV generation setup.

(2 standard deviations) of the full scale (Fig. 4). The variance is even less for the 0.2 m region upstream of the reactor center, where products are sampled for TOF-MS (referred to as the MS sampling region). Temperature profiles were measured for nominal temperatures of 300-800 K and 10-50 Torr of flowing helium with a 1 s residence time from the gas inlet to outlet.

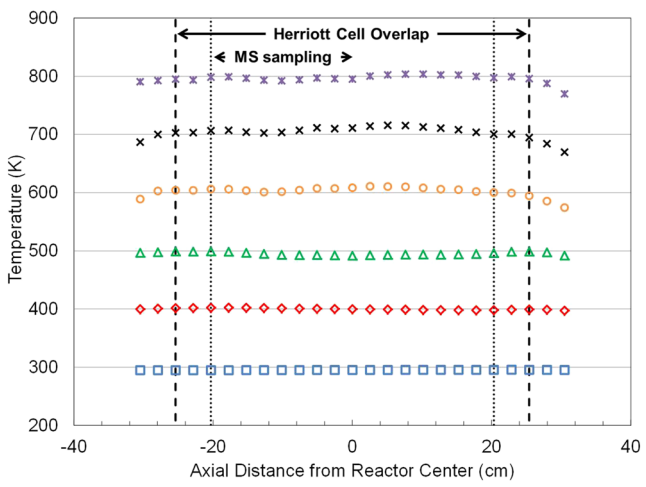


FIG. 4. Representative axial centerline temperature profiles measured at nominal $T$'s of 300-800 K. The gas residence time in the Herriott cell overlap region is ~300 ms, while for the MS sampling region, it is ~50 ms.

All of the measured profiles were of similar quality as those in Fig. 4.

The current accessible $T$,$P$-range of this apparatus is quoted as 300-800 K and 1-50 Torr (Table I). The lower bound for $T$ is set by room temperature (no controlled cooling capability currently), and the lower bound for P is set by the accuracy of the pressure gauge controlling the butterfly valve. Of course, a different P-gauge could be used with a lower range, so the real limit is set by the density of gas needed to observe the chemistry of interest. The high-$T$ and high-$P$ limits are closely related, as they are currently set by the maximum power output of the short pre-heater before it burns out. Both upper bounds have additional constraints as well. For $T$, many of the chemical precursors that will photodissociate at 266 or 355 nm (wavelengths of photolysis laser used) such as iodobenzene, $C_6H_5I$, will also start to thermally dissociate significantly on a 1 s time scale (reactor residence time) as $T$ approaches 1000 K. This is the main reason that none of the flash photolysis/PIMS experiments summarized in Table I exceed 1050 K. For $P$, as discussed by Osborn *et al.*,[36] less than 10 Torr is desirable to allow fast (<1 ms) radial diffusion to "smooth out" any non-uniformity in the photolytically generated radical concentration due to a non-uniform beam profile. However, this is mainly a concern if kinetics (i.e., time-dependence) are to be measured by time-resolved MS, in which case transport delays (including diffusion to the MS sampling region within

the reactor) can and should be minimized to 10-100 $\mu$s.[3,36] In our case, however, kinetics are measured by LAS, which does not require any physical sampling of the reactive mixture (hence no transport delays) and which is also mostly insensitive to local concentration variations under pseudo-first-order conditions. Therefore, as long as the primary reaction products can be clearly resolved by TOF-MS before secondary reactions take over, a lower time resolution is acceptable, allowing both LAS and TOF-MS measurements up to 50 Torr in the current apparatus.

The gas in the photolyzed region in the center of the reaction cell was sampled through a "funnel-shaped" pinhole, adapted from Wyatt *et al.*,[60] with a 275 $\mu$m diameter at the narrowest point. We found that this geometry was necessary to prevent excessive wall reactions inside the pinhole during sampling. The gas is driven continuously through the pinhole by a large pressure gradient. Typical pressures inside the reaction cell ranged from 10 to 50 Torr, with 10 Torr found to be a good balance for most experiments. Typical pressures in the low-vacuum chamber outside the reaction cell were around $10^{-5}$-$10^{-4}$ Torr, and a very large 2000 L/s Leybold turbomolecular pump was used to handle the relatively high gas load of a continuously sampled system while still achieving low enough pressures. The roughly 5-7 orders of magnitude difference in pressure between the reaction cell and the low-vacuum chamber was required to supersonically expand the gas sampled from the pinhole. The three purposes of sampling the reactor gases through such an expansion were already outlined in the Introduction.

After exiting the pinhole (or nozzle in free-jet parlance), the gas rapidly expands and attains speeds greater than the speed of sound; i.e., it becomes supersonic and has a Mach number greater than 1. This supersonic zone immediately outside the pinhole is called the *zone of silence*, and it is within this zone that the gas is both cooled and nearly collision-free. To extract the gas from this zone, a 1.0 or 2.0 mm diameter Model 16.3 Beam Dynamics conical skimmer was placed about 1.0-2.0 mm away from the pinhole, depending on the position of the reaction cell. This optimal distance was calculated using the empirical equations of Miller.[31] The skimmer eliminated the slower and less-cooled regions of gas away from the axis of the zone of silence, and it created a molecular beam to transport the gas sample continuously to the ionization region of the mass spectrometer. The skimmer also provided an additional reduction in pressure by reducing the gas load to the high-vacuum chamber where the gas sample is ionized. This reduction in pressure decreased the amount of VUV photoionization light losses due to absorption by the scattered background gas, and it brought the high-vacuum pressure to a level suitable for the use of an electron impact ionization source, with which our TOF-MS is also equipped. Finally, the reduction of pressure due to the skimmer indirectly allowed the TOF-MS to be used with greater pressures in the reaction cell by decreasing the pressure at the TOF-MS snout and thus the pressure within the TOF-MS.

### B. Herriott multiple-pass laser absorption

As noted above, the geometry of the reaction cell was designed to sample the photolyzed region via a small pinhole without disturbing the ability to simultaneously probe the same region using the Herriott multiple-pass laser absorption technique. The photolyzed region is defined by the region through which the photolysis beam passes, the diameter of which is matched to the ID of the central portion of the reactor (1.6 cm) using a pair of telescoping lenses. Typically, we use the fourth harmonic (266 nm) output of a Nd:YAG laser (1064 nm fundamental) for photolysis, although the third harmonic (355 nm) can also be used. The maximum output of the current photolysis laser at 266 nm is ~100 mJ per pulse, which corresponds to ~$10^{17}$ photons per pulse. As explained in Sec. III A, only ~$10^{12}$ cm$^{-3}$ of radicals are needed to achieve sufficient signal-to-noise (S/N) for both LAS and PI TOF-MS detection and therefore a negligible portion of the photolysis beam is attenuated, while passing through the reactor. The repetition rate of the photolysis laser is set to match the residence time in the reaction cell: typically 1 s or 1 Hz.

The probe laser is composed of a Spectra Physics Tsunami Ti:Sapphire laser, a Spectra Physics Millennia Xs diode pump laser, and a Spectra Physics GWU doubler/tripler module. The Tsunami Ti:Sapphire laser is a mode-locked laser that produces 1.2 ps FWHM pulses of light at 80 MHz. The Millennia Xs pump laser is a 10 W 532 nm continuous wave (CW) diode-pumped laser. The output of the Ti:Sapphire laser is tunable from 690 to 1080 nm with the use of two optic sets, and the wavelength is measured using either an Ocean Optics HR 2000+ spectrometer (790-950 nm with 0.12 nm resolution) or an Ocean Optics USB 2000 spectrometer (~1 nm resolution). The Ti:Sapphire laser frequency can be either doubled to 345-540 nm or tripled to 230-360 nm using the GWU module. Because the temporal resolution of the Ti:Sapphire laser is very high, the frequency bandwidth has a relatively large value, 13 cm$^{-1}$. However, many free radicals have even broader absorption features in the UV-visible range; in these cases, the relatively low probe resolution does not adversely affect the signal-to-noise (S/N). For example, allyl,[50] benzyl,[51] phenyl,[52] peroxy,[15,62] and vinyl[11] radicals, as well as the simplest Criegee intermediate[49] and iodine monoxide,[12] have all been identified as detectable species with the current LAS setup[22] because they are all known to absorb broadly and strongly (cross sections range from $10^{-19}$ to $10^{-18}$ cm$^2$) in the UV-visible range. Experimentally, all of the aforementioned species have been observed using the current LAS apparatus.[6,9,24] If a chemical system becomes of interest in the future that requires better spectral resolution, either the current probe laser could be modified to output 10 ps pulses with a 10× narrower bandwidth or an entirely different probe laser could be used. The root mean square of the relative intensity noise in the probe laser is ~0.0001 from 1 Hz to 1 MHz, which is the main source of random noise for the LAS technique.[22]

The Herriott multi-pass setup is shown in Fig. 2 as the green beams and in Fig. S1 of the supplementary material. The photolysis beam enters from the left and passes through the middle of the hole at the center of each mirror. Prior to entering the reactor, the probe beam is reshaped by a set of cylindrical lenses to correct for astigmatism and mode-matched to the Herriott cell by a spherical lens.[22] The probe beam then enters from the right side of the cell though a slit in the mirror.

The probe beam reflects between the mirrors, intersecting the photolysis beam in the overlap region multiple times before exiting via a slit in the left mirror. By using separate optical elements for the photolysis and probe beams, there is less opportunity for spurious signals to appear due to either scattered photolysis light reaching the probe laser detectors or transient heating of the probe laser optics by the photolysis pulse. The Herriott mirrors are spherical with an 800 mm radius of curvature and a 380-550 nm 99% reflective coating on a clear BK7 substrate. Figure S2 of the supplementary material shows the pattern of reflections observed behind one of the mirrors when the Herriott cell is well-aligned. The reference and signal beam intensities are both measured by Thorlabs DET110 Silicon detectors on the inlet and outlet side of the reactor, respectively.

The characteristics of the Herriott multiple-pass laser system have been extensively studied, and equations to describe the system have been published by others.[21,38,55] The overlap path length of the probe laser beam within the photolyzed region is calculated from the formulas given by Herriott *et al.*[21] and Trutna and Byer[55] for the special case of a circular cell (the original formulas are given in a general form for an elliptical geometry). For a typical setup, the overlap of a single-pass of the Herriott cell with the photolyzed region is 0.7 ± 0.15 m and the total number of passes is 39 such that the total overlap path length is 28 ± 6 m. The uncertainty is from propagation of error.

We also use a New Focus Vortex TLB-6025 CW diode laser centered at 1315.28 nm to probe the concentration of iodine (I) atoms made during the photolysis of iodinated precursor molecules such as vinyl iodide and phenyl iodide.[7] This beam passes through the slits in the Herriott mirrors in a single pass counter to the probe beam and is focused onto a Thorlabs DET10C InGaAs detector. The path length of the I atom laser is ~70 cm, which is sufficient to measure the 3 → 4 hyperfine transition of the I atom.[19]

At either end of the apparatus are two custom vacuum crosses used to house the Herriott mirrors in semi-custom mirror mounts (crosses shown in both Figs. 1 and 5). The crosses allow control of the tilt (both horizontal and vertical), axial translation, and slit angle of the Herriott mirrors while under vacuum in order to facilitate alignment. The photolysis, probe, and I atom lasers enter and exit through these crosses, passing through a window positioned at Brewster's angle to ensure minimal back-reflections. Brewster's angle, defined here as the angle of incidence that best propagates p-polarized 266 nm light through the UV-fused silica windows, was calculated to be 56°.

### C. Photoionization

Typically, roughly 10 electron-volts (eV) of energy are required to ionize most stable organic molecules.[10] Thus, high-energy radiation in the VUV range is required to photoionize most molecules. To generate this type of radiation, the third harmonic (frequency-tripled) 355 nm output of an Nd:YAG laser is frequency tripled again in a xenon/argon gas mixture to produce the ninth harmonic 118.2 nm (10.487 eV) wavelength.[29] To accomplish the conversion of 355 nm photons into 118.2 nm photons, the collimated 355 nm beam from a pulsed Quantel Brilliant Nd:YAG laser (~50 mJ/pulse, 5 ns pulse width) is focused into a 1:10 Xe:Ar gas mixture

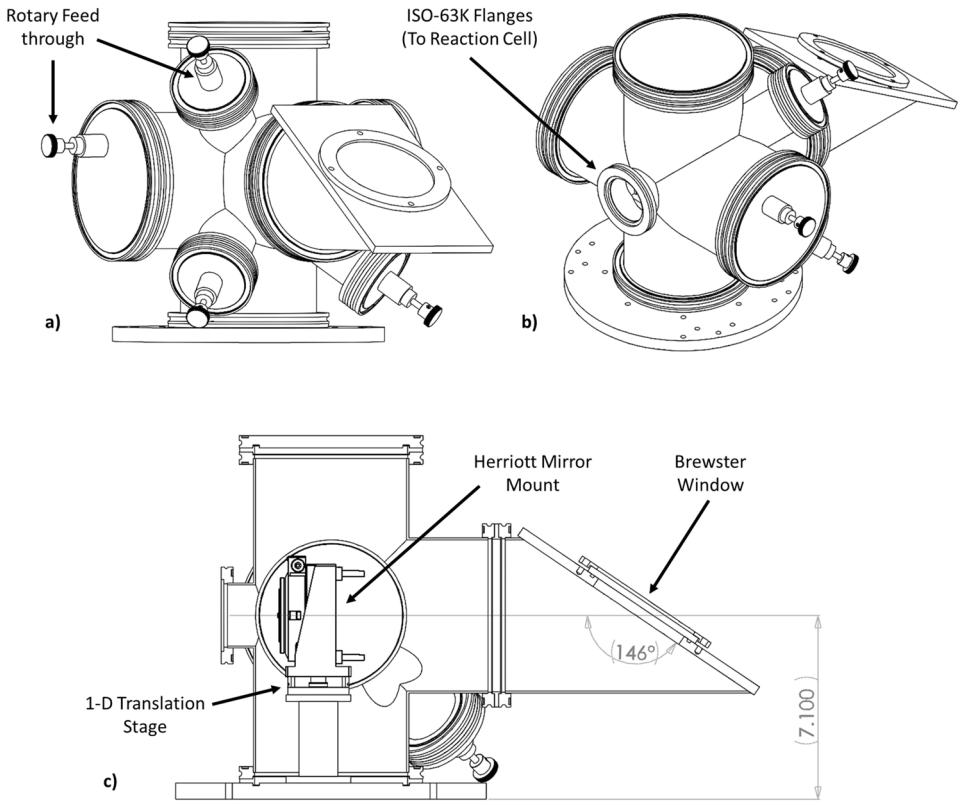


FIG. 5. Custom Herriott cross assembly with semi-custom Herriott mirror mounts inside shown from (a) the side furthest from the vacuum chamber, (b) the side close to the vacuum chamber, and (c) in cross sectional view with relevant dimensions shown (in inches).

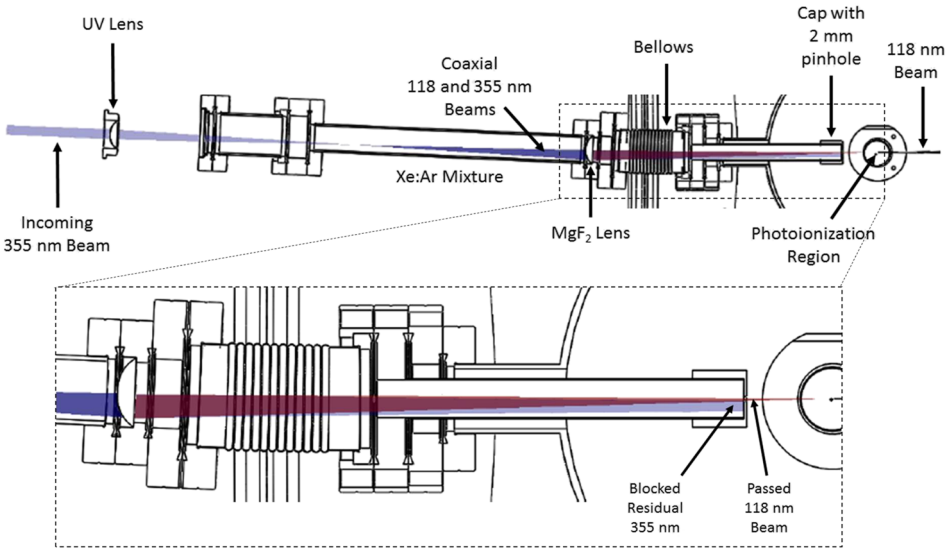


FIG. 6. Top cross sectional view of the VUV generation setup showing the separation of the residual 355 nm radiation from the desired 118 nm radiation for photoionization.

at 80-100 Torr using a plano-convex UV-fused silica lens (21.6 cm focal length), as shown in Figs. 3 and 6. The beam must be focused into the gas mixture because the nonlinear conversion process by which the frequency-tripling occurs can only take place at sufficiently high power densities ($W/cm^2$), as is the case for most nonlinear optical conversion processes.[56]

After the 118.2 nm radiation is generated, it passes through an $MgF_2$ lens along with the residual 355 nm radiation. As shown in Fig. 6, the two beams are aligned 5 mm off-axis of the $MgF_2$ lens such that the lens spatially separates the two wavelengths of radiation, like a prism, due to their different indices of refraction in $MgF_2$.[59] The incoming beams are also at ~2.5° angle with respect to the normal of the vacuum chamber in order for the 118.2 nm beam to focus in the photoionization region. By contrast, the 355 nm beam is not refracted sufficiently by the $MgF_2$ lens and is therefore not aligned with the photoionization region. Finally, after passing through the $MgF_2$ lens, the two beams propagate through a tube terminated by a cap with a 2 mm hole drilled in its center. The 118.2 nm beam passes through the 2 mm hole, whereas the 355 nm beam is blocked by the cap. In this manner, only the 118.2 nm radiation is permitted in the photoionization region. If both beams are allowed in the photoionization region, we observed species in the mass spectrum with ionization energies well above 10.5 eV, such as He, as well as unexpected fragments, such as vinyl cations from vinyl iodide fragmentation (11.3 eV appearance energy[40]). After switching to the $MgF_2$-lens-as-prism approach described above and used by many other researchers,[53,61] both the helium and the unexpected fragment signals disappeared.

The residual 118.2 nm light was partially reflected onto a NIST aluminum oxide-coated VUV photodiode using an uncoated elliptical flat as the partial reflector. Only a portion of the 118.2 nm beam was reflected onto the VUV photodiode surface, instead of the entire beam, to avoid exceeding the damage threshold of the photodiode. The VUV photodiode signal can be used to normalize each corresponding TOF-MS spectrum for shot-to-shot fluctuations in VUV intensity. However, normal averaging of the TOF-MS spectra for around 100 shots without explicitly correcting the shot-to-shot VUV intensity fluctuations was found to be sufficient to get acceptable statistics. Furthermore, if normalization is desired, it is better to normalize to another TOF-MS signal, for example, one of the internal standard signals present in small concentration or another transient product. In this manner, fluctuations from other sources (e.g., photolysis laser power, molecular beam density, detector sensitivity) can be accounted for as well.

The Kore TOF-MS used in the apparatus is also equipped with an electron impact ionization source. This $e^-$-impact source essentially consists of a filament in front of a slit with a plate behind it held at a specific adjustable voltage. The default setting of 70 V provides 70 eV of electron impact ionization energy. While time-resolved electron impact experiments can be performed, the data acquisition hardware was not optimized for such experiments. That is, data could only be collected at the repetition rate of the photolysis laser (<10 Hz), even though electron-impact experiments could be conducted at much high repetition rates (e.g., 50 kHz) by pulsing the TOF-MS independently. This would allow the time evolution of the mass spectra to be observed in real time, much like what is done with any other continuous ionization source. Electron impact spectra are also difficult to interpret, and the relatively high ionization energy causes many of the parent ions for each molecule to fragment into smaller ions. Often, a single fragmentation peak arises from a number of parent peaks, making deconvolution of the mass spectra necessary and usually difficult. However, the electron impact source was a useful diagnostic tool for our system. For species that do not ionize when using the 118.2 nm (10.487 eV) light, such as $O_2$, we can observe them using electron impact ionization, to check for a leak for example. Also, when troubleshooting issues, such as a lack of signal, we can use the electron impact source to determine if the VUV ionization setup is the problem or if the tuning of the TOF-MS is the problem.

### D. Time-of-flight mass spectrometer

A schematic of the Kore TOF-MS used in the apparatus is shown in Fig. S3 of the supplementary material. The cations produced by either photoionization or electron impact ionization are accelerated into the snout of the TOF-MS by the electric field applied between the extraction plate (held at ground) and the TOF-MS components (held at negative voltages). For the case of photoionization, the extraction plate voltage is held constant, while for the case of electron impact ionization (which is continuous), the extraction voltage is pulsed to give a time t = 0 for each time-of-flight mass spectrum. For photoionization, the time of the laser pulse is time t = 0 for each mass spectrum. After entering the snout (or entrance aperture) of the TOF-MS, the ions are spatially focused by an ion lens, which consists of a Faraday cage with precisely machined curved edges. Thereafter, the ion trajectories are steered using a set of X and Y deflector plates. After passing through the field-free region (FFR), the ions are reflected and focused both spatially and temporally using a reflectron. The reflectron consists of a retard plate to slow the ions and a stack of plates with a steep gradient of voltages to reflect the ions. Finally, after traveling back through the FFR region, the ions strike the discrete dynode electron multiplier detector. The signal from the detector is then amplified using an analog pre-amplifier when using photoionization (relatively large packets of ions for each m/z) or using a digital pre-amplifier when using electron impact ionization (single-ion counting for each m/z, i.e., the Poisson limit). The signal from the analog pre-amplifier is digitized and averaged over ~100 photolysis shots using a 2.5 GHz (set to 1.0 GS/s) Tektronix DPO7254 oscilloscope. The signal from the digital pre-amplifier is histogrammed using a Kore time-to-digital converter. The amplifiers can be swapped relatively easily, but they cannot be used together at the same time.

### E. Timing and data acquisition

Figures 7 and 8 depict schematically the timing and data acquisition for both detection techniques (LAS and PI TOF-MS). The timing of the entire experiment is controlled using a BNC 575 digital delay generator. For the LAS experiment, only the firing of the photolysis laser requires an external trigger. The probe and I atom lasers also used in the LAS experiment are quasi-cw and cw, respectively, such that neither requires an external trigger. The intensity of the Ti:Sapphire laser is measured by a pair of photodiodes before and after passing through the reaction cell, and a differential amplifier is used to subtract the former signal from the latter, resulting in a significant reduction in noise.[22] The I atom laser intensity is measured only at the exit of the reactor as differential amplification was found unnecessary in that case, although the resulting signal is amplified by 500 times. The photolysis laser flash, detected by another photodiode, is used as the trigger for a 1 GHz oscilloscope (Lecroy 6100A Waverunner) that records the intensity decays of the probe and I atom lasers. The signal is averaged on the oscilloscope, typically for ~100 photolysis shots (~1 min acquisition time at 1 Hz), before being sent to the "LabView PC" for storage and further processing on the "Analysis PC."

For the PI TOF-MS experiment, there are several components that require external triggers. In addition to the photolysis laser, the photoionization laser also requires triggering. The delay of the photoionization laser trigger is adjusted by LabVIEW, via the delay generator, to scan through different reaction times. The delay generator can also be used to trigger

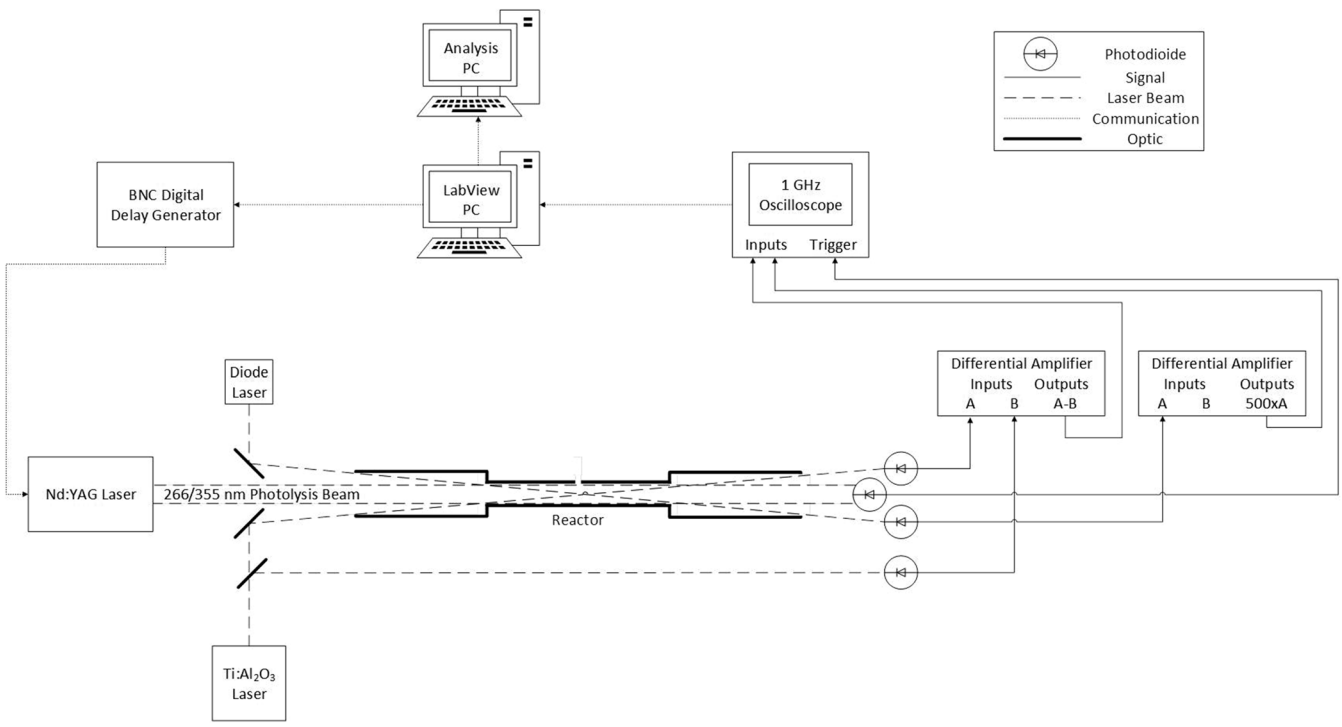


FIG. 7. Schematic of timing and data acquisition for the LAS experiment.

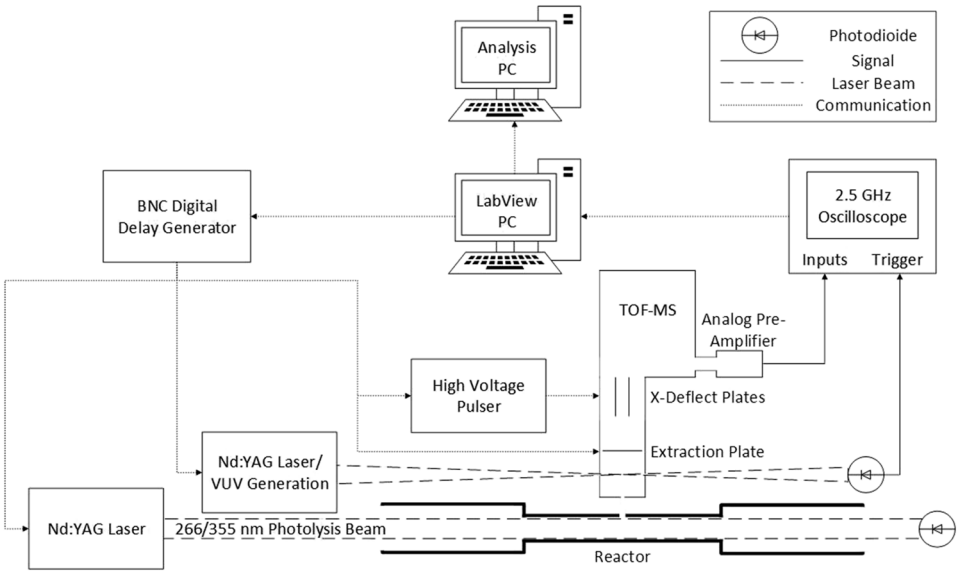


FIG. 8. Schematic of timing and data acquisition for the PI TOF-MS experiment.

the high-voltage extraction plates of the TOF-MS, which is necessary when a continuous ionization source is used, such as an electron gun or atomic resonance lamp. The other channels of the delay generator are used to trigger the high-voltage pulser (DEI PVX-4140) that is connected to the X/Y deflection plates of the TOF-MS (Fig. S3 of the supplementary material) in order to direct large packets of ions from background gases away from the detector and avoid saturating the detector signal. The firing of the photoionization laser, as detected by a VUV photodiode, is used to trigger a 2.5 GHz oscilloscope (Tektronix DPO7254) that records the amplified mass spectrum. This oscilloscope is also used to verify the delay time between the photolysis and photoionization shots, corresponding to the current reaction time being probed by TOF-MS. The delay time between the firing of the two lasers is precise within 10 ns, well below the resolution of the TOF-MS experiment due to molecular beam sampling (Sec. III B). After averaging for ~100 shots (~1 min), the spectrum acquired on the oscilloscope is sent to the LabView and Analysis PC's for storage and further processing.

The entire experiment, including the temperature and pressure of the reaction cell, the gas flows, the TOF-MS calibration, and the data acquisition, is controlled using a custom LabVIEW program. The data taken using the instrument are analyzed using a custom MATLAB program. This program allows mass spectra from multiple reaction times to be loaded simultaneously and the various m/z peaks assigned and integrated automatically. It also allows simple pseudo-first order, second-order, and biexponential fits to be applied to the LAS data. This program is useful for on-the-fly evaluation of the data being taken, saving time by allowing problems to be identified and fixed before proceeding.

## III. RESULTS

### A. Sensitivity

The sensitivity of the laser absorption spectrometry (LAS) portion of the apparatus was previously characterized by Ismail.[22] Ismail determined that the use of differential amplification greatly reduced the noise in the Ti:Sapphire probe laser signal, as the subtraction of the reference beam taken before the absorption cell removed most of the systematic fluctuations in the probe laser intensity. Most of the intensity fluctuations in the probe beam were due to intensity fluctuations from the Spectra Physics Millennia Xs diode pump laser power supply. Thus, the noise in the absorption signals for the new apparatus could likely be improved further by either upgrading the power supply of the Millennia pump laser or replacing it entirely with a state-of-the-art low-noise pump laser.

Another significant source of noise in the LAS experiment is thermal lensing, which is the movement of laser beams due to refraction of the beam from thermal gradients. Because the reaction cell is heated and some of the components around the apparatus radiate heat, the laser beams pass through a number of transient thermal gradients. These transient thermal gradients refract the laser beam randomly, causing its position to wobble slightly. For the probe beam that is reflected by the Herriott mirrors and passes through a steep thermal gradient within the reaction cell many times, the degree of random movement due to thermal lensing can be quite pronounced (e.g., ~1-2 mm of movement in the final beam at high reaction cell temperatures). Thermal lensing can be manifested in the LAS measurements as either random "wiggles" and baseline shifts in the trace or as completely spurious "signals" due to transient heating of the photolyzed region during the photolysis shot. Averaging can reduce random noise introduced by thermal lensing, while background subtraction of absorbance traces with bath gas only can eliminate spurious signals. The problem of thermal lensing is made worse by greater thermal gradients and by passing through gases with higher polarizabilities. The refractive index of a gas is a function of its polarizability, and gases with higher polarizabilities tend to exhibit greater changes in the refractive index as the temperature is changed. Therefore, helium was typically used as a buffer gas for most experiments due to its relatively low polarizability. While other inert gases such as argon or nitrogen

would have served equally well as a diluent gas, these gases possess greater polarizabilities than helium and thus result in higher levels of problem-causing thermal lensing.

Even with residual noise from the pump laser and noise from thermal lensing, it is still possible to detect transient absorption signals as small as 0.0001.[23] For the 30 m overlap path length used to determine this limit by Ismail *et al.*, this detection limit corresponds to a cross section weighted concentration of $\sigma_i C_i = 3.3 \times 10^{-8}$ cm$^{-1}$. For a phenyl radical, which has an absorption cross section of $3.6 \times 10^{-19}$ cm$^2$,[52] this corresponds to a minimum concentration of $\sim 10^{11}$ molecules/cm$^3$.

The sensitivity of the PI TOF-MS portion of the apparatus was characterized using a custom calibration gas mixture. The calibration gas mixture, which contained seven species diluted in helium (propene, 1,3-butadiene, furan, benzene, cyclohexane, toluene, and heptane) with known concentrations and known photoionization cross sections, was also used to calibrate the conversion of time-of-flight to m/z in the TOF-MS. The signal for any given species $i$ in the TOF-MS is given by the following equation:

$$S_i = \sigma_{PI,i} R_i C_i, \tag{2}$$

where $S$ is the signal (integrated m/z peak area), $\sigma_{PI}$ is the photoionization cross section at 10.487 eV, $R$ is the mass discrimination factor, and $C$ is the concentration in the reaction cell.

Equation (2) is a simplification of the complete relationship between $S$ and $C$[36] but will suffice for our purposes. The mass discrimination factor is an instrument-dependent factor that accounts for any systematic differences in signal due to differences in the gas sampling and the detection efficiencies for each species. Technically, every species has its own mass discrimination factor, but typically this parameter is mostly a function of the mass-to-charge ratio (m/z) and is not strongly dependent on the exact identity and features of the species being detected.[10] The mass discrimination factor for the PI TOF-MS was measured by the calibration gas signal during an experiment (phenyl radical + propene at 707 K and 10 Torr, Sec. III D) and is shown in Fig. 9. Note that of the seven calibration gas species, only four could be used in this analysis because the remaining three (propene, benzene, and toluene) overlapped with some other species or precursor impurities in the reactor during the experiment. The mass discrimination factor was fit to a power law

$$R_i = A\left[\frac{m}{z}\right]^b, \tag{3}$$

which is the functional form typically used to match R. $A$ is essentially a lumped conversion factor between the cross section weighted concentration and TOF-MS signal [Eq. (2)] and $b$ accounts for any dependence on m/z. The fit in Fig. 9 uses $b = 0.57$, similar to the square root dependence on m/z empirically observed before.[36] Interestingly, without excess propene present in the reactor, no dependence of $R_i$ on m/z was observed across the entire calibration gas range (42-100 amu). Nonetheless, for the combustion applications of current interest to us, a heavy hydrocarbon like propene will often be present in the reaction mixture. Therefore, the best approach

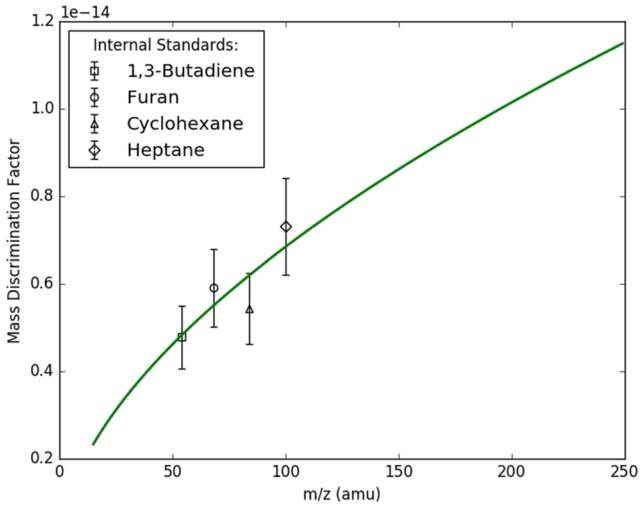


FIG. 9. Mass discrimination factors measured (markers) at 707 K, 10 Torr during a phenyl radical + propene experiment (Sec. III D). Error bars are from 15% uncertainty in photoionization cross sections. The line is a power law fit.

to quantifying $R_i$ (needed for subsequent product quantification) is to fit the measured signals *in situ* of a small known concentration of calibration gas, such as in Fig. 9.

The detection limit for the PI TOF-MS was estimated by measuring signals from the species in the calibration gas mixture using various levels of dilution and comparing them to the noise in the baseline of the mass spectra after averaging 100 times (background noise). To account for the fact that each species has a different photoionization cross section and thus gives a different signal for the same concentration, S/N is plotted versus the cross section weighted concentration ($\sigma_i C_i$, Fig. 10). Plotting versus $\sigma_i C_i$ effectively collapses all of the data onto a single line (accounting for at least 15% cross section uncertainty), which was fit using the least-squares method. Defining the minimum discernable signal to correspond to S/N = 3, the detection limit for the PI TOF-MS is estimated to be $\sigma_i C_i = 2 \times 10^{-8}$ cm$^{-1}$. In terms of a typical organic molecule

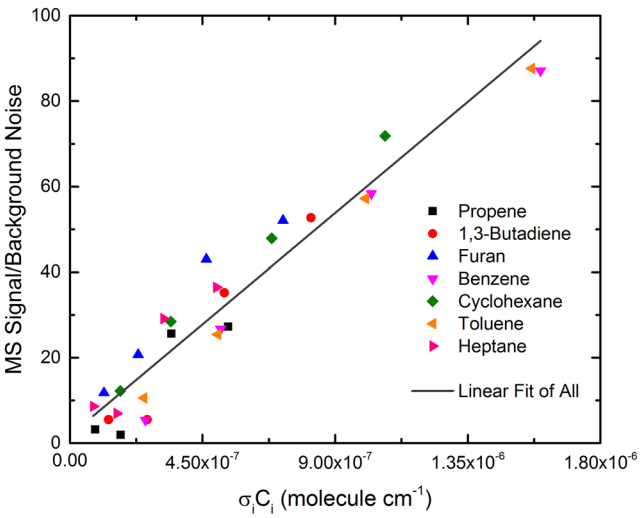


FIG. 10. Calibration gas measurements used to determine the detection limit of PI TOF-MS at 10 Torr and 300 K.

such as propene (~10 MB photoionization cross section) or a radical such as phenyl (~17 MB[46]), this detection limit corresponds to ~$10^9$ molecules/cm$^3$, about two orders of magnitude lower than the LAS detection limit. Similar detection limits were measured at both 10 and 50 Torr.

This measured detection limit can be rationalized through some simple calculations. First, the detection limit is defined as the point at which only one ion is generated per photoionization laser shot (single ion counting limit). Second, typical 355–118 nm conversion efficiencies are only 0.0001%[56] such that for 50 mJ pulse$^{-1}$ of 355 nm input energy we should generate ~$10^{11}$ photons of VUV. Third, we assumed that the free jet density drops by two orders of magnitude relative to the reactor density (reactor pressure ~10 Torr) before being skimmed 2 mm from the reactor pinhole, after which the molecular beam has minimal spread in the transverse direction such that the overlap path length between the VUV and molecular beams is ~1 mm.[17] Finally, we assumed a typical photoionization cross section of $10^{-17}$ cm$^2$ (10 MB), which gives a detection limit of $10^9$ molecules cm$^{-3}$ in the reactor, in excellent agreement with our measured detection limit. Typically we operate at conditions such that the TOF-MS signals for important products of a photolytically initiated reaction are 1-2 orders of magnitude above the detection limit and therefore well above the single ion counting regime.

However, this detection limit is an optimistic estimate because it was measured using stable species with only helium bath gas. Radical species will be harder to detect due to wall losses. Additionally, in a real experiment, there will often be a large organic molecule (e.g., propene) also present in high concentration that tends to lower the S/N for a given $\sigma_i C_i$ due to both attenuation of VUV photons and a decrease in the molecular beam density for a heavier carrier gas.[33] Therefore, initial radical concentrations during actual experiments were typically ~$10^{12}$ molecules/cm$^{-3}$ such that the various stable products formed have concentrations ~$10^{11}$ and give MS S/N's of at least 10 (above single ion counting limit) even in the presence of a heavy excess reagent. This initial radical concentration is also ideal for LAS as it is 10× that detection limit, but not so high that radical-radical recombination will become a significant problem on our experimental time scale (a typical high-pressure bimolecular rate coefficient of ~$1 \times 10^{-10}$ cm$^3$ molecule$^{-1}$ s$^{-1}$ for vinyl[24] and phenyl radicals[54]).

Another feature of Fig. 10 worth commenting on is the linear dependence of S/N on $C_i$ for a given species, such as benzene or toluene. It is reassuring that in the S/N range of 10-100 where most products were quantified the MS detector is within its linear response regime.

### B. Time and mass resolution

Because the Ti:Sapphire laser is actually pulsed at 80 MHz, or every 12.5 ns, the fastest possible reaction time scale that can be measured is limited to 10× this value in order to have at least 10 points to fit during the decay. For a pseudo-first order system, this time scale corresponds to a maximum reaction rate of $k' = 8 \times 10^6$ s$^{-1}$. However, this upper-limit is constrained further by considering the effect of RC electronics on the signal during data acquisition. Specifically, the Stanford Research System SR560 pre-amplifier used to take the difference between the laser intensity before and after the reaction cell (increasing the sensitivity of the LAS experiment by orders of magnitude, as discussed in Sec. III A) has a maximum 1 MHz bandwidth. Therefore, the fastest measurable $k'$ for the LAS experiment is $1 \times 10^6$ s$^{-1}$, as we have previously noted.[7] Similarly, the slowest radical decay that we have managed to observe with LAS also exhibited signal distortion due to the electronic data acquisition process.[7] In this case, the pre-amplifier, which had a high-pass filter of 0.03 Hz, was not the problem, but rather the oscilloscope to which the signal was AC coupled also acted as a high pass filter with an RC time constant of 65 ms. Therefore, we estimate the slowest measurable $k'$ without significant electronic signal distortion as 50 s$^{-1}$. For transient species that are smaller or more reactive than the iodine atom, their slowest decays will likely be limited by some other physical process, such as diffusion out of the probe volume or wall reaction before this limit is reached. Thus, the absolute greatest range of first order rate coefficients that can be measured using the LAS method with this instrument is estimated as the following:

$$50\,\mathrm{s}^{-1} < k' < 1 \times 10^6\,\mathrm{s}^{-1}.$$

This four decade range of measurable $k'$ values is ideal for overall kinetics measurements, where it is desirable to measure pseudo-first-order decays over as wide a range as possible.

The range of kinetic time scales that can currently be measured using the time-resolved PI TOF-MS technique are very limited compared to the LAS technique. Although the BNC 575 delay generator has sub-nanosecond time resolution and can control the relative timing of the photolysis and the photoionization lasers to well within their ~10 ns laser pulse durations, the time resolution of the PI TOF-MS data is constrained to much longer time scales by other factors. In particular, the fastest possible measurement time scales are limited by transport delays during molecular beam sampling that include diffusion to the sampling pinhole, flow through the pinhole, and transport via the supersonic expansion to the ionization region of the TOF-MS. The effect of effusive and supersonic sampling on kinetic measurements has been extensively characterized theoretically by Moore and Carr[32] and Taatjes,[48] and experimentally, it has been verified that processes as fast as 100 $\mu$s can be resolved by both effusive[3] and supersonic[36] expansions. In our case, the rate-limiting transport step is actually diffusion within the reactor due to radial inhomogeneities in the photolysis beam, a delay that becomes more acute at higher $P$. In order to estimate the overall effect of all transport processes on the observed PI TOF-MS time-resolution, the simple, one-parameter model of Baeza-Romero *et al.* for transport of species $i$ from the reactor to the ionization region was adapted,[3]

$$\frac{dS_\mathrm{i}}{dt} = k_{sampling}\left(R_i \sigma_{PI,i} C_i(\mathrm{t}) - S_\mathrm{i}\right), \tag{4}$$

where $k_{sampling}$ is a first order rate-coefficient used as a fit parameter to describe the rate of transport both to and from the ionization region and $S_i$, $R_i$, $\sigma_{PI,i}$, and $C_i$ have the same

definitions as before (MS signal, mass discrimination factor, photoionization cross section, and concentration in the reactor). Baeza-Romero *et al.* showed for a variety of $C_i$(t) functional forms that Eq. (4) can be used to accurately fit for kinetic processes with pseudo-first-order rate coefficients, $k'$, up to half of $k_{sampling}$. For example, if $C_i$(t) is a step function at $t = 0$ that changes by $\Delta C_{i,0}$ (can be either positive or negative) to a constant value, then Eq. (4) can be solved to give an analytical equation for the change in $S_i$(t), $\Delta S_i$(t),

$$\Delta S_i(t) = R_i \sigma_i \Delta C_{i,0}(1 - e^{-k_{sampling} t}). \quad (5)$$

Therefore, if we photolytically generate some species in the reaction cell that has a step concentration profile, $k_{sampling}$ can be determined by fitting the TOF-MS signal observed for this species to Eq. (5). The positive jump in the I atom MS signal (m/z = 127 amu) following photodissociation of $C_6H_5I$ was used for this purpose (Fig. 11), although a more complicated form of $C_I$(t) was used that accounts for subsequent reactions of the I atom necessitating numerical solution of Eq. (4).

Figure 11 compares two different models of sampling: instantaneous ($k_{sampling} \rightarrow \infty$) and fit ($k_{sampling}$ = 750 $s^{-1}$). Clearly the instantaneous model is not suitable, but it is helpful for visualizing what the profile should look like (what it *does* look like inside of the reactor) and how sampling effects distort that behavior. Over the course of conducting experiments on the phenyl radical + propene system (Sec. III D), $k_{sampling}$ was fit over a range of $T$, $P$ and reactor gas composition, from which it was observed that $k_{sampling}$ is typically ~1000 $s^{-1}$ (such as in Fig. 11) and decreases with increasing P and propene concentration, $C_{C_3H_6}$. The last two observations are consistent with diffusion within the reactor being the rate-limiting transport step, as both increasing $P$ and $C_{C_3H_6}$ will inhibit diffusion. From this analysis, the fastest process that could be measured reliably with time-resolved TOF-MS is ~500 $s^{-1}$ (half of $k_{sampling}$) giving a time-resolution of ~1 ms.

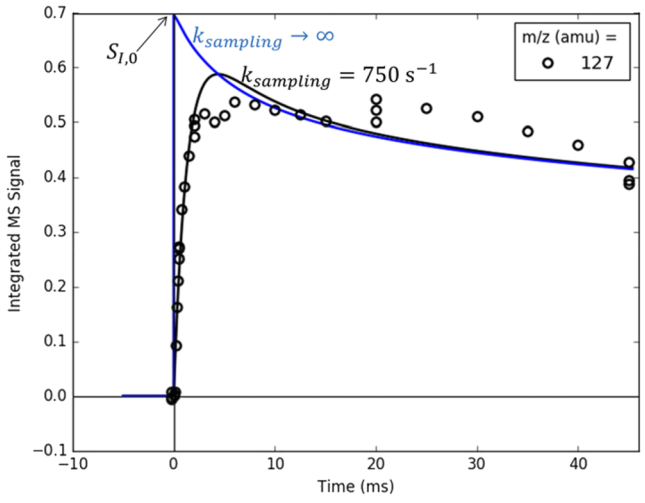


FIG. 11. Measured (circles) time-resolved PI TOF-MS profile of the I atom at 127 amu, following 266 nm photodissociation of iodobenzene in the presence of $C_3H_6$ at 707 K, 10 Torr. The lines are two different models of MB sampling: instantaneous (blue) and delayed by fitting a $k_{sampling}$ of 750 $s^{-1}$. Back-extrapolation of $S_{I,0}$ for initial radical concentration quantification is also shown.

Diffusion is slower in our reactor compared to either Osborn or Blitz for several reasons: 1. We are operating at higher pressures (≥10 Torr) in order to observe the relatively slow chemistry of interest to us. 2. In order to fit the Herriott cell, our reactor is relatively wide (1.6/3.6 cm ID) and long (~1 m from the Brewster inlet window to pinhole) such that the photolysis beam must be expanded and propagated over a long length, which will tend to create hot spots in the beam. 3. Given the greater reactor length, slight misalignments of the photolysis beam can also cause the region directly adjacent to the pinhole not to be completely illuminated. 4. We are probing bulkier molecules (e.g., an iodine atom in Fig. 11 and aromatic molecules in Sec. III D) with smaller diffusivities. Of course this resolution can and should be improved down to a 10-100 $\mu$s time scale, for instance, by using a reactor $P$ < 10 Torr when possible or working to improve the radial uniformity of the photolysis beam. Nonetheless, for the purpose of primary product branching quantification, a 1 ms time resolution is sufficient so long as primary products can still be distinguished from later generation products, which was found to be the case for the phenyl radical + propene system described in Sec. III D. This is especially true considering that the LAS portion of the apparatus already has $\mu$s time resolution and as a non-intrusive detection technique is preferable for kinetic measurements.

The slowest $k'$ that can be measured with TOF-MS is limited by convective transport of the reactive gas out of the MS sampling region (Fig. 4). For a typical total residence time of 1 s, the residence time in the MS sampling region is ~50 ms. Therefore, the range of pseudo-first-order rate coefficients that can be measured using the PI TOF-MS method is as follows:

$$20 < k' < 500\ s^{-1}.$$

Depending on the identity of the species being sampled for PI TOF-MS, the lower bound on $k'$ could be higher due to wall reaction loss. Clearly this is a very restrictive range that is not suitable for overall kinetics measurements, but it is sufficient for extracting quantitative product branching by PI TOF-MS, as shown in Sec. III D.

The mass resolution of the PI TOF-MS, $m/\Delta m$, is ~400 as measured by fitting a gaussian to each of the seven peaks in the calibration gas mass spectrum and taking the full width at half maximum, FWHM, of the fit as $\Delta m$ (see Fig. 12). This resolution is more than sufficient to distinguish chemical species with m/z values separated by 1 amu over the m/z range of interest, 1-200 amu. For example, in Fig. 12, the $^{13}C$ isotopologue for each species is clearly resolvable. The current cation flight time is relatively short (~20 $\mu$s for m/z = 200 amu); therefore, depending on the origin of the broadening, it might be possible to achieve higher mass resolution by extending the length of the flight path.

Table II summarizes the sensitivity and resolution of both parts of the apparatus. Using the phenyl radical as an example, the PI TOF-MS detection limit is ~2 orders of magnitude lower than it is for LAS. As already mentioned, for a typical initial radical concentration of $1 \times 10^{12}$ molecules $cm^{-3}$, the LAS S/N will be ~10, and the various products that are subsequently formed with concentrations of ~$1 \times 10^{11}$ molecules $cm^{-3}$ will appear in the TOF-MS with S/N up to ~100. Despite

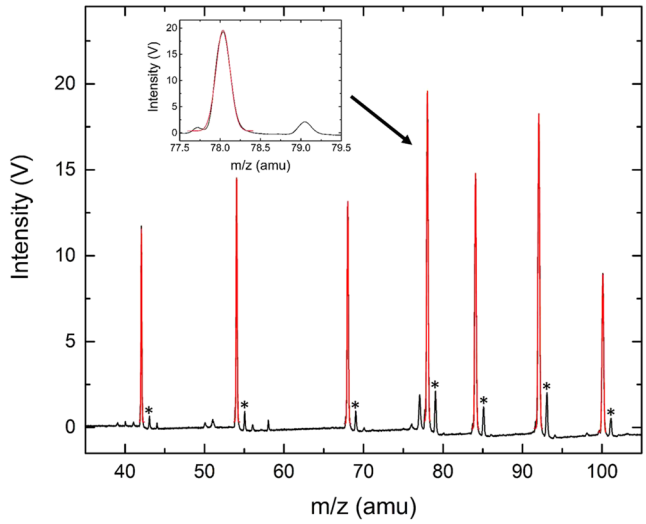


FIG. 12. Representative mass spectrum of calibration gas with gaussian fits to each peak in order to estimate **Δm**. Calibration gas consists of propene (m/z = 42 amu), 1,3-butadiene (54), furan (68), benzene (78), cyclohexane (84), toluene (92), and n-heptane (100). There is a fragment of an iodobenzene impurity ($C_6H_5I$) at 77 amu and an acetone impurity at 58 amu. Other unidentified peaks are likely accumulated impurities in the reactor. Asterisks denote $^{13}C$ peaks of calibration gas.

its lower sensitivity (currently), LAS can measure a much wider range of $k'$. The advantage of combining both experiments is clear: LAS can be used to measure the kinetics of one species' decay with very high time-resolution, whereas PI TOF-MS can measure the appearance of many species at once albeit with lower time-resolution. Even if the time resolution of PI TOF-MS detection is too slow to resolve $k'$, it can still be used to accurately quantify product branching fractions. Finally, other than wall reactions, all of the limitations in Table II are technical rather than fundamental, and therefore, they all have technical solutions. As an example, routes to improve the fastest TOF-MS $k'$ have already been discussed, while the slowest TOF-MS $k'$ (due to convection out of the MS-sampling region) could be extended by simply increasing the gas residence time. As another example, the detection limit of LAS could drop by an order of magnitude by increasing the number of probe laser passes accordingly, such as in cavity ringdown spectrometry,[37] or with an astigmatic Herriott cell.[30] It also bears mentioning that although LAS in this apparatus currently uses a picosecond Ti:Sapphire laser, there is no reason that another UV/visible laser with a narrower bandwidth could be directly used instead to allow more selective radical detection. For example, a dye laser tuned to the 308 nm absorbance band of the hydroxyl radical, OH, a very important oxidant in atmospheric and combustion chemistry.[34] While these examples are helpful for highlighting possible directions for future modification/improvement, the current iteration of the apparatus is perfectly capable of achieving the original goal: simultaneous measurements of overall kinetics with high time-resolution and quantitative primary product branching. The expected accuracy and precision of these measurements are discussed in Sec. III C.

### C. Precision and accuracy of kinetics measurements

Besides verifying that the LAS/PI TOF-MS apparatus *can* be used to measure overall kinetics and product branching, it is equally important to know *how precisely* and *accurately* those quantities can be measured and *why*. Table III summarizes the answers to these questions.

For overall kinetics measured by LAS, the precision can be very high and is limited primarily by the amount of random noise induced by thermal lensing, which depends in turn on the particular conditions of the experiment. In the near-absence of thermal lensing, precision is limited by the uncertainty in fitting $k'$, which is $<\pm 0.1\%$ as we have shown previously[6] due to the high density of data points for a given absorbance decay. However, the accuracy is limited by ±5% systematic uncertainty in the mass flow controller (MFC) calibrations used to control gas flow rates, which translates into ±10% systematic uncertainty in the excess reagent concentrations needed to convert $k'$ into the bimolecular rate coefficient of interest, $k$. If each MFC was specifically calibrated for the gas that it is used to flow during an experiment, then the accuracy could improve to ±1%. For our purposes, 10% accuracy in $k$ is adequate.

For product branching measured by PI TOF-MS, the precision is ~7% due to fluctuations in both the photoionization and photolysis laser energies. This was determined by comparing replicate measurements of both photolysis-dependent and independent MS signals. For photolysis-independent signals (i.e., calibration gas), the highest precision measured was ~2% (one standard deviation), whereas for photolysis-dependent signals (styrene product in Sec. III D), it was ~7% at best. The accuracy is limited to ±15% due to systematic uncertainties in photoionization cross sections (PICS) needed for quantification. This is a well-known limitation of MS-based quantification techniques, but perhaps if relative PICS were measured with the same instrument and then applied to a measured product signal ratio, the resulting product branching

TABLE II. Summary of LAS/PI TOF-MS apparatus characterization.

| | Detection limit | | Slowest measurable $k'$ | | Fastest measurable $k'$ | | |
|---|---|---|---|---|---|---|---|
| Detection technique | $\sigma_i C_i$ ($cm^{-1}$) | (Phenyl radical) ($cm^{-3}$)[a] | Value ($s^{-1}$) | Cause | Value ($s^{-1}$) | Cause | Mass resolution |
| LAS | $3 \times 10^{-8}$ | $1 \times 10^{11}$ | 50 | High-pass RC filter of the oscilloscope | $1 \times 10^{6}$ | Low-pass RC filter of the differential pre-amplifier | ... |
| PI TOF-MS | $2 \times 10^{-8}$ | $1 \times 10^{9}$ | 20 | Convection/wall reactions | 500 | Diffusion to pinhole/MB sampling | 400 |

[a]Absorption and photoionization cross sections of the phenyl radical at 504.8 nm and 10.5 eV taken from the studies of Tonokura *et al.*[52] and Sveum *et al.*,[46] respectively.

TABLE III. Summary of precision and accuracy for both overall kinetics and product branching measurements using LAS and PI TOF-MS, respectively.

| | Precision | | Accuracy | |
|---|---|---|---|---|
| Measurement | Value (±%, 1σ) | Cause | Value (±%) | Cause |
| Overall kinetics by LAS | <0.1[a] | Fitting $k'$ | 10 | Mass flow controller calibrations |
| Product branching by PI TOF-MS | 7 | Fluctuations in VUV/photolysis lasers | 15 | Photoionization cross sections |

[a]Without thermal lensing.

ratio would be known with much greater accuracy because of a large cancellation of systematic uncertainties.

This brief analysis represents a best-case scenario estimate, while Sec. III D demonstrates for a real system how precisely and accurately overall kinetics and product branching can actually be measured using LAS/PI TOF-MS.

### D. Demo system: Phenyl radical + propene

The results shown below are a subset of the total set of phenyl radical + propene ($C_6H_5$ + $C_3H_6$) experiments conducted with the LAS/PI TOF-MS apparatus. The full data set with detailed analysis and discussion is the subject of another publication.[9] Figure 13 shows representative time-resolved mass spectra obtained under conditions where $C_6H_5$ + $C_3H_6$ occurs: photodissociation of iodobenzene, $C_6H_5I$, in the presence of $C_3H_6$. For convenience, the spectra are divided into low (m/z = 75-125 amu) and high (125-250 amu) ranges (no transient signal observed <77 amu). All of the expected primary products channels of $C_6H_5$ + $C_3H_6$ are observed in the low range: hydrogen-abstraction (benzene, $C_6H_6$ at 78 amu; $C_3H_5$ at 41 amu is not visible due to overlap with a large $C_3H_6$ fragment) and radical addition followed by methyl radical,

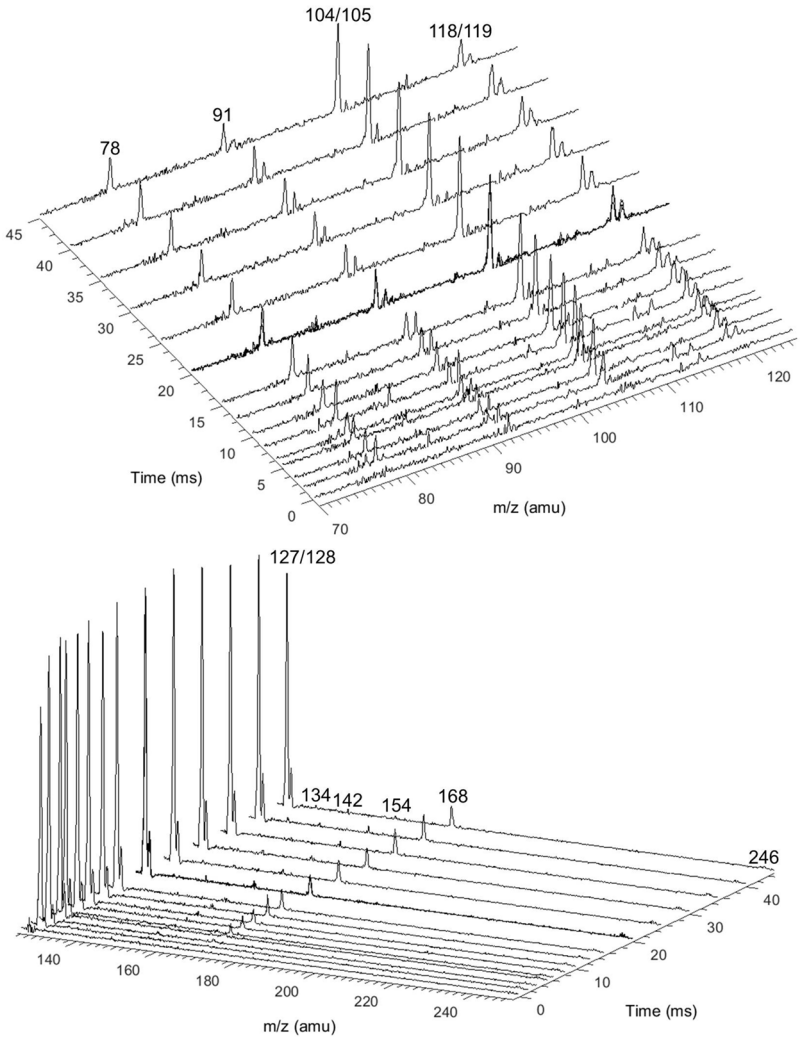


FIG. 13. Background-subtracted, time-resolved mass spectra at m/z range where primary phenyl radical + propene products appear (70-125 amu, top) and a higher m/z range where mostly parent cations of iodide-containing species appear (125-250 amu). Measured at 707 K and 10 Torr with $C_{C_3H_6} = 7.4 \times 10^{15}$ and $C_{C_6H_{5,0}} = 1 \times 10^{12}$ molecules cm$^{-3}$. Only positive changes are shown. Each spectrum was averaged over 100 shots (~2 min at 1 Hz).

$CH_3$, loss (styrene, $C_8H_8$, at 104 amu) or hydrogen, H, loss (phenylpropene isomers, $C_9H_{10}$, at 118 amu). Although the signal at 119 amu corresponds to the same m/z as a stabilized $C_6H_5$ + $C_3H_6$ radical adduct ($C_9H_{11}$), the time-dependence observed is not consistent with a radical (too long-lived), and, by detailed modeling, it was revealed to be a fragment of a secondary product (next paragraph). An unexpected primary product is also observed at 91 amu, nominally corresponding to the benzyl radical, $C_7H_7$. Through a combination of quantum calculations, rate theory, and automatic mechanism generation, it was determined that the benzyl radical is formed from $C_6H_5$ + $C_3H_6$ via a previously unreported "aromatic-catalyzed" 1,2-H-migration with ethene, $C_2H_4$, as a co-product. This example demonstrates that qualitative observations made with time-resolved PI TOF-MS can be of great value, even for a system such as $C_6H_5$ + $C_3H_6$ that has already been studied extensively by CMB[1,25,63] and thermal experiments,[20,37,64] as well as theoretical calculations.[27,57] The other "signals" observed in the low range of the mass spectrum are due to fluctuations of the internal standard gases and impurities (cyclohexane at 84 amu, toluene at 92 amu, n-heptane at 100 amu, and phenyl chloride at 112 and 114 amu) and are not correlated with reaction time.

The signals in the high m/z range correspond to the I atom and various secondary products. Many of the secondary products arise from recombination of the I atom with another radical present in the reactor including H (128 amu), $CH_3$ (142 amu), $C_3H_5$ (168 amu), and $C_9H_{11}$ (246 amu). Although secondary and higher generation products are generally undesirable, using TOF-MS they can at least be observed and included in the analysis. For example, the presence of a transient signal at the parent m/z of $C_9H_{11}I$ (248 amu) quickly led us to the realization that the signal at 119 amu was mostly a fragment of $C_9H_{11}I$. Subsequent quantitative analysis reinforced this conclusion. The other secondary products observed are from phenyl self-recombination (biphenyl, 154 amu) and recombination of $C_9H_{11}$ with other radicals: $CH_3$ (134 amu) and $C_3H_5$ (160 amu, not discernable in Fig. 13).

The signals observed in Fig. 13 were all integrated for further quantitative analysis, and Fig. 14 shows the results only for the primary $C_6H_5$ + $C_3H_6$ products. The lines are model predictions based on the calculations of Kislov *et al.*[27] Quantitatively, styrene (104 amu) was measured as the dominant product by ~3-4× in agreement with predictions. The dominance of styrene is also consistent with the other experimental studies of $C_6H_5$ + $C_3H_6$ product branching, where styrene was found to be the major product over a wide temperature and collision energy range. The other measured products match the predictions as well. The insensitivity of the measured product branching to the concentration of propene, precursor, and radical, as well as the photolysis laser fluence was confirmed by control experiments.

Also shown in Fig. 14 is a simultaneous measurement of $C_6H_5$ decay by the 505.3 nm LAS on a much shorter time scale: 5 ms compared to the 45 ms PI TOF-MS time scale. The time-resolution of LAS is more than sufficient to resolve the pseudo-first-order decay of $C_6H_5$, which is also in good agreement with the predictions The decay rate of $C_6H_5$ was measured with LAS over a range of propene concentrations

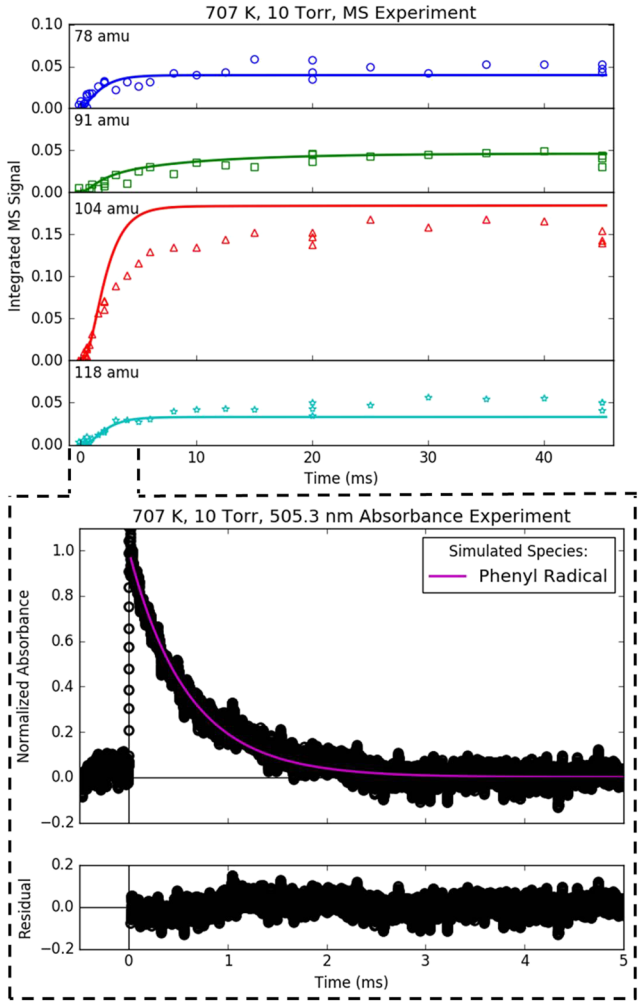


FIG. 14. Measured (markers) and predicted (lines) primary products of phenyl radical + propene quantified by MBMS (top) and decay of the phenyl radical measured simultaneously by the 505.3 nm LAS (bottom). Measured at 707 K and 10 Torr with $C_{C_3H_6} = 7.4 \times 10^{15}$ and $C_{C_6H_{5,0}} = 1 \times 10^{12}$ molecules $cm^{-3}$. The LAS trace was averaged over 200 shots (~4 min at 1 Hz). Predictions are based on the calculations of Kislov *et al.*[27] Primary products are nominally benzene (78 amu), benzyl radical (91), styrene (104), and phenylpropene isomers (118 amu), although other species also contribute at these m/z's.[9]

from 300 to 700 K. From these data, the overall kinetics of $C_6H_5$ + $C_3H_6$ were measured and found to be in agreement with the cavity ring-down spectrometry measurements of Park and Lin.[37]

Regarding the uncertainty in these measurements, the overall kinetics of $C_6H_5$ + $C_3H_6$ were measured with 10% accuracy at various temperatures due to systematic uncertainty in the $C_3H_6$ concentration as discussed in Sec. III C and in other publications.[6,8] The primary product branching ratios, however, have much higher uncertainty due to both lower precision and accuracy. As shown in Fig. 15, after only a few milliseconds, the ratio of the 78–104 amu signal, $S_{C_6H_6}/S_{C_8H_8}$, appears to have reached a steady state value of 0.31 ± 0.04 (one standard deviation uncertainty). This random uncertainty of ~15% is greater than the 7% precision quoted in Table III because the 78 amu signal is near the detection limit where background noise starts to make a noticeable contribution.

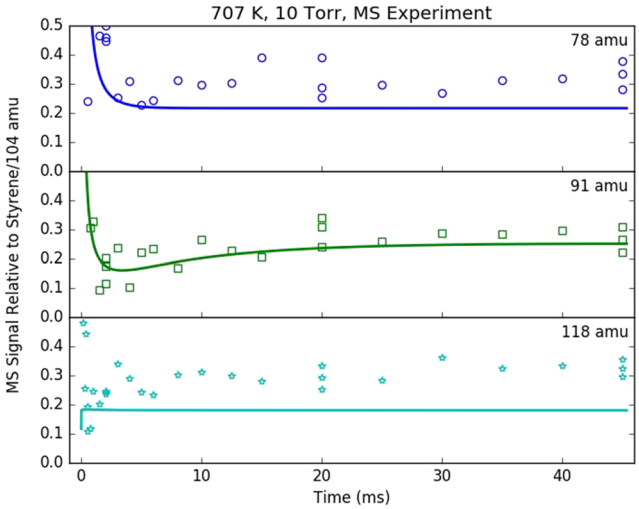


FIG. 15. Measured (markers) and predicted (lines) primary products of phenyl radical + propene quantified by MBMS at 707 K and 10 Torr with $C_{C_3H_6} = 7.4 \times 10^{15}$ and $C_{C_6H_{5,0}} = 1 \times 10^{12}$ molecules cm$^{-3}$. Both measured and predicted results are plotted relative to the 104 amu/styrene signal at each time point. Predictions are based on the calculations of Kislov *et al.*[27]

Although the concentration of $C_6H_6$ is ~$10^{11}$ cm$^{-3}$, which is well above the detection limit of $10^9$ cm$^{-3}$ quoted in Table II for PI TOF-MS, the added presence of ~6% $C_3H_6$ attenuates the MS signal by absorbing VUV photons and reducing the molecular beam density as already noted in Sec. III A, effectively raising the detection limit. By contrast, the steady-state 104 amu signal is much higher, as seen in Fig. 14, and is measured with ~7% precision. In order to convert the signal ratios to concentration ratios, photoionization cross sections, $\sigma_{PI}$, must be applied,

$$\frac{C_{C_6H_6}}{C_{C_8H_8}} = \frac{S_{C_6H_6}}{S_{C_8H_8}} \times \frac{\sigma_{PI,C_8H_8}}{\sigma_{PI,C_6H_6}}. \quad (6)$$

$\sigma_{PI}$ for $C_6H_6$ is 31.8 Megabarns (Mb) with ±6.4 systematic uncertainty,[10] and for $C_8H_8$, it is 42.9 ± 4.3 Mb.[65] Combining both random and systematic uncertainties, the measured product branching ratio between $C_6H_6$ and $C_8H_8$ is 0.47 ± 0.19, which represents the competition between the H-abstraction and $CH_3$-loss channels in the $C_6H_5$ + $C_3H_6$ system at the given conditions. As seen from this simple exercise, systematic uncertainty in $\sigma_{PI}$ dominates the overall product branching uncertainty, and as already mentioned in Sec. III C, this uncertainty could be reduced by measuring relative $\sigma_{PI}$.

## IV. CONCLUSIONS

A flash photolysis apparatus that combines multiple-pass laser absorption spectrometry (LAS) for overall kinetics measurements with time-resolved photoionization time-of-flight mass spectrometry (PI TOF-MS) for quantitative product branching was described, characterized, and tested for a representative chemical system. In order to accommodate both detection techniques simultaneously, unique reactor and vacuum chamber designs were necessary. The current temperature and pressure range of the apparatus is 300-800 K and 1-50 Torr, respectively. The PI TOF-MS is two orders of magnitude more sensitive than LAS such that an initial radical concentration of ~$1 \times 10^{12}$ molecules cm$^{-3}$ is optimal for both aspects of the experiment. LAS is ideal for quantification of overall kinetics because the decay of one species can be measured with high time resolution, whereas PI TOF-MS is preferred for product branching quantification because multiple products can be measured simultaneously albeit with lower time resolution. Simultaneous measurement of both the total rate and product branching ratios on a single photolysis flash has significant advantages over the conventional approach of measuring these quantities separately: the availability of both types of data helps with interpretation and simplifies detection of problems due to interferences or impurities, and the measurements are insensitive to fluctuations in photolysis flash intensity. The capability of the new apparatus was demonstrated for the chemically interesting phenyl radical + propene system.

## SUPPLEMENTARY MATERIAL

See supplementary material for a schematic and picture of the Herriott multiple-pass cell, and a schematic of the KORE TOF-MS.

## ACKNOWLEDGMENTS

Dr. Mark Blitz hosted J.E.M. in his lab several years ago and has been a valuable resource ever since. Professor Vadim Knyazev allowed Z.J.B. to visit his lab and has also provided many useful discussions since then. We are grateful for many helpful discussions with Professor Robert W. Field and members of his research group and also for their willingness to lend us equipment. The primary source of funding for the multi-year development and demonstration of this unique instrument has been the U.S. Department of Energy's Basic Energy Sciences division, recently through its Gas Phase Chemical Physics program (Grant No. DE-0014901) and prior to 2015 through its Energy Frontier Research Center for Combustion Science (Grant No. DE-SC0001198). The phenyl + propene experiments shown here as an example were funded by SABIC. The George Harrison Spectroscopy Laboratory, which was financially supported by the National Science Foundation, provided the Ti:sapphire probe laser. ExxonMobil provided funding for the bowtie reactor.

[1] Albert, D. R., Todt, M. A., and Davis, H. F., "Crossed molecular beams studies of phenyl radical reactions with propene and trans-2-butene," J. Phys. Chem. A **117**, 13967–13975 (2013).
[2] Antonov, I. O., Zádor, J., Rotavera, B., Papajak, E., Osborn, D. L., Taatjes, C. A., and Sheps, L., "Pressure-dependent competition among reaction pathways from first- and second-$O_2$ additions in the low-temperature oxidation of tetrahydrofuran," J. Phys. Chem. A **120**, 6582–6595 (2016).
[3] Baeza-Romero, M. T., Blitz, M. A., Goddard, A., and Seakins, P. W., "Time-of-flight mass spectrometry for time-resolved measurements: Some developments and applications," Int. J. Chem. Kinet. **44**, 532–545 (2012).
[4] Blitz, M. A., Goddard, A., Ingham, T., and Pilling, M. J., "Time-of-flight mass spectrometry for time-resolved measurements," Rev. Sci. Instrum. **78**, 034103 (2007).
[5] Buckingham, G. T., Ormond, T. K., Porterfield, J. P., Hemberger, P., Kostko, O., Ahmed, M., Robichaud, D. J., Nimlos, M. R., Daily, J. W., and Ellison, G. B., "The thermal decomposition of the benzyl radical in a heated micro-reactor. I. Experimental findings," J. Chem. Phys. **142**, 044307 (2015).

[6]Buras, Z. J., Elsamra, R. M. I., Jalan, A., Middaugh, J. E., and Green, W. H., "Direct kinetic measurements of reactions between the simplest Criegee intermediate $CH_2OO$ and alkenes," J. Phys. Chem. A **118**, 1997–2006 (2014).

[7]Buras, Z. J., Elsamra, R. M. I., and Green, W. H., "Direct determination of the simplest Criegee intermediate ($CH_2OO$) self reaction rate," J. Phys. Chem. Lett. **5**, 2224–2228 (2014).

[8]Buras, Z. J., Dames, E. E., Merchant, S. S., Liu, G., Elsamra, R. M. I., and Green, W. H., "Kinetics and products of vinyl + 1,3-butadiene, a potential route to benzene," J. Phys. Chem. A **119**, 7325–7338 (2015).

[9]Buras, Z. J., Chu, T.-C., Jamal, A., Yee, N. W., Middaugh, J. E., and Green, W. H., "Phenyl radical + propene: A prototypical reaction surface for aromatic-catalyzed 1,2-hydrogen-migration and subsequent resonance-stabilized radical formation," Phys. Chem. Chem. Phys. **20**, 13191–13214 (2018).

[10]Cool, T. A., Wang, J., Nakajima, K., Taatjes, C. A., and McLlroy, A., "Photoionization cross sections for reaction intermediates in hydrocarbon combustion," Int. J. Mass Spectrom. **247**, 18–27 (2005).

[11]DeSain, J. D., Jusinski, L. E., and Taatjes, C. A., "Ultraviolet photochemistry of trichlorovinylsilane and allyltrichlorosilane: Vinyl radical ($HCCH_2$) and allyl radical ($H_2CCHCH_2$) production in 193 nm photolysis," Phys. Chem. Chem. Phys. **8**, 2240–2248 (2006).

[12]Dillon, T. J., Tucceri, M. E., Hölscher, D., and Crowley, J. N., "Absorption cross-section of IO at 427.2 nm and 298 K," J. Photochem. Photobiol., A **176**, 3–14 (2005).

[13]Eskola, A. J. and Timonen, R. S., "Kinetics of the reactions of vinyl radicals with molecular oxygen and chlorine at temperatures 200-362 K," Phys. Chem. Chem. Phys. **5**, 2557–2561 (2003).

[14]Eskola, A. J., Wojcik-Pastuszka, D., Ratajczak, E., and Timonen, R. S., "Kinetics of the reactions of $CH_2Br$ and $CH_2I$ radicals with molecular oxygen at atmospheric temperatures," Phys. Chem. Chem. Phys. **8**, 1416–1424 (2006).

[15]Fahr, A., Laufer, A. H., Krauss, M., and Osman, R., "Gas phase absorption spectrum and cross sections of vinylperoxy ($C_2H_3O_2$) radical," J. Phys. Chem. A **101**, 4879–4886 (1997).

[16]Fockenberg, C., Bernstein, H. J., Hall, G. E., Muckerman, J. T., Preses, J. M., Sears, T. J., and Weston, R. E., "Repetitively sampled time-of-flight mass spectrometry for gas-phase kinetics studies," Rev. Sci. Instrum. **70**, 3259–3264 (1999).

[17]Goldsmith, C. F., *Predicting Combustion Properties of Hydrocarbon Fuel Mixtures* (Massachussetts Institute of Technology, Cambridge, 2010).

[18]Gu, X. and Kaiser, R. I., "Reaction dynamics of phenyl radicals in extreme environments: A crossed molecular beam study," Acc. Chem. Res. **42**, 290–302 (2009).

[19]Ha, T.-K., He, Y., Pochert, J., Quack, M., Ranz, R., Seyfang, G., and Thanopoulos, I., "Absolute integrated band strength and magnetic dipole transition moments in the $^2$P3/2 → $^2$P1/2 fine structure (with hyperfine structure) transition of the iodine atom: Experiment and theory," Ber. Bunsen-Ges. Phys. Chem. **99**, 384–392 (1995).

[20]Hefter, H. J., Hecht, T. A., and Hammond, G. S., "Radical attack on propylene as studied by electron spin resonance," J. Am. Chem. Soc. **94**, 2793–2797 (1972).

[21]Herriott, D., Kogelnik, H., and Kompfner, R., "Off-Axis paths in spherical mirror interferometers," Appl. Opt. **3**, 523–526 (1964).

[22]Ismail, H., *Addition and Recombination Reactions of Unsaturated Radicals Using a Novel Laser Kinetics Spectrometer* (Massachusetts Institute of Technology, Cambridge, 2008).

[23]Ismail, H., Goldsmith, C. F., Abel, P. R., Howe, P.-T., Fahr, A., Halpern, J. B., Jusinski, L. E., Georgievskii, Y., Taatjes, C. A., and Green, W. H., "Pressure and temperature dependence of the reaction of vinyl radical with ethylene," J. Phys. Chem. A **111**, 6843–6851 (2007).

[24]Ismail, H., Abel, P. R., Green, W. H., Fahr, A., Jusinski, L. E., Knepp, A. M., Zádor, J., Meloni, G., Selby, T. M., Osborn, D. L., and Taatjes, C. A., "Temperature-dependent kinetics of the vinyl radical ($C_2H_3$) self-reaction," J. Phys. Chem. A **113**, 1278–1286 (2009).

[25]Kaiser, R. I., Parker, D. S. N., Goswami, M., Zhang, F., Kislov, V. V., Mebel, A. M., Aguilera-Iparraguirre, J., and Green, W. H., "Crossed beam reaction of phenyl and D5-phenyl radicals with propene and deuterated counterparts-competing atomic hydrogen and methyl loss pathways," Phys. Chem. Chem. Phys. **14**, 720–729 (2012).

[26]Kanofsky, J. R., Lucas, D., Pruss, F., and Gutman, D., "Direct identification of the reactive channels in the reactions of oxygen atoms and hydroxyl radicals with acetylene and methylacetylene," J. Phys. Chem. **78**, 311–316 (1974).

[27]Kislov, V. V., Mebel, A. M., Aguilera-Iparraguirre, J., and Green, W. H., "Reaction of phenyl radical with propylene as a possible source of indene and other polycyclic aromatic hydrocarbons: An *ab initio*/RRKM-ME study," J. Phys. Chem. A **116**, 4176–4191 (2012).

[28]Knepp, A. M., Meloni, G., Jusinski, L. E., Taatjes, C. A., Cavallotti, C., and Klippenstein, S. J., "Theory, measurements, and modeling of OH and $HO_2$ formation in the reaction of cyclohexyl radicals with $O_2$," Phys. Chem. Chem. Phys. **9**, 4315–4331 (2007).

[29]Lockyer, N. P. and Vickerman, J. C., "Single photon ionisation mass spectrometry using laser-generated vacuum ultraviolet photons," Laser Chem. **17**, 139–160 (1997).

[30]McManus, J. B., Zahniser, M. S., and Nelson, D. D., "Dual quantum cascade laser trace gas instrument with astigmatic Herriott cell at high pass number," Appl. Opt. **50**, A74–A85 (2011).

[31]Miller, D., "Free jet sources," in *Atomic and Molecular Beam Methods*, edited by Scoles, G. (Oxford University Press, Oxford/New York, 1988).

[32]Moore, S. B. and Carr, R. W., "Molecular velocity distribution effects in kinetic studies by time-resolved mass spectrometry," Int. J. Mass Spectrom. Ion Phys. **24**, 161–171 (1977).

[33]Morse, M. D., "2-Supersonic beam sources," in *Experimental Methods in the Physical Sciences*, edited by Dunning, F. B. and Hulet, R. G. (Academic Press, 1996), Vol. 29, pp. 21–47.

[34]Nasir, E. F. and Farooq, A., "A shock-tube study of the CO + OH reaction near the low-pressure limit," J. Phys. Chem. A **120**, 3924–3928 (2016).

[35]Ng, C.-Y., "Vacuum ultraviolet spectroscopy and chemistry by photoionization and photoelectron methods," Annu. Rev. Phys. Chem. **53**, 101–140 (2002).

[36]Osborn, D. L., Zou, P., Johnsen, H., Hayden, C. C., Taatjes, C. A., Knyazev, V. D., North, S. W., Peterka, D. S., Ahmed, M., and Leone, S. R., "The multiplexed chemical kinetic photoionization mass spectrometer: A new approach to isomer-resolved chemical kinetics," Rev. Sci. Instrum. **79**, 104103 (2008).

[37]Park, J., Nam, G. J., Tokmakov, I. V., and Lin, M. C., "Experimental and theoretical studies of the phenyl radical reaction with propene," J. Phys. Chem. A **110**, 8729–8735 (2006).

[38]Pilgrim, J. S., Jennings, R. T., and Taatjes, C. A., "Temperature controlled multiple pass absorption cell for gas phase chemical kinetics studies," Rev. Sci. Instrum. **68**, 1875–1878 (1997).

[39]Senosiain, J. P., Klippenstein, S. J., and Miller, J. A., "The reaction of acetylene with hydroxyl radicals," J. Phys. Chem. A **109**, 6045–6055 (2005).

[40]Shuman, N. S., Ochieng, M. A., Sztáray, B., and Baer, T., "TPEPICO spectroscopy of vinyl chloride and vinyl iodide: Neutral and ionic heats of formation and bond energies," J. Phys. Chem. A **112**, 5647–5652 (2008).

[41]Slagle, I. R. and Gutman, D., "Kinetics of polyatomic free radicals produced by laser photolysis. 5. Study of the equilibrium $CH_3 + O_2 = CH_3O_2$ between 421 and 538 C," J. Am. Chem. Soc. **107**, 5342–5347 (1985).

[42]Slagle, I. R., Yamada, F., and Gutman, D., "Kinetics of free radicals produced by infrared multiphoton-induced decompositions. 1. Reactions of allyl radicals with nitrogen dioxide and bromine," J. Am. Chem. Soc. **103**, 149–153 (1981).

[43]Smith, G. P., Tao, Y., and Wang, H., Foundational Fuel Chemistry Model Version 1.0 (FFCM-1), http://nanoenergy.stanford.edu/ffcm1.

[44]Stein, S. E., Walker, J. A., Suryan, M. M., and Fahr, A., "A new path to benzene in flames," Symp. (Int.) Combust. **23**, 85–90 (1991).

[45]Stone, D., Blitz, M., Daubney, L., Howes, N. U. M., and Seakins, P., "Kinetics of $CH_2OO$ reactions with $SO_2$, $NO_2$, NO, $H_2O$ and $CH_3CHO$ as a function of pressure," Phys. Chem. Chem. Phys. **16**, 1139 (2013).

[46]Sveum, N. E., Goncher, S. J., and Neumark, D. M., "Determination of absolute photoionization cross sections of the phenyl radical," Phys. Chem. Chem. Phys. **8**, 592–598 (2006).

[47]Sztáray, B., Voronova, K., Torma, K. G., Covert, K. J., Bodi, A., Hemberger, P., Gerber, T., and Osborn, D. L., "CRF-PEPICO: Double velocity map imaging photoelectron photoion coincidence spectroscopy for reaction kinetics studies," J. Chem. Phys. **147**, 013944 (2017).

[48]Taatjes, C. A., "How does the molecular velocity distribution affect kinetics measurements by time-resolved mass spectrometry?," Int. J. Chem. Kinet. **39**, 565–570 (2007).

[49]Ting, W.-L., Chen, Y.-H., Chao, W., Smith, M. C., and Lin, J. J., "The UV absorption spectrum of the simplest Criegee intermediate $CH_2OO$," Phys. Chem. Chem. Phys. **16**, 10438–10443 (2014).

[50]Tonokura, K. and Koshi, M., "Absorption spectrum and cross sections of the allyl radical measured using cavity ring-down Spectroscopy: The $\tilde{A} \leftarrow \tilde{X}$ band," J. Phys. Chem. A **104**, 8456–8461 (2000).

[51]Tonokura, K. and Koshi, M., "Cavity ring-down spectroscopy of the benzyl radical," J. Phys. Chem. A **107**, 4457–4461 (2003).
[52]Tonokura, K., Norikane, Y., Koshi, M., Nakano, Y., Nakamichi, S., Goto, M., Hashimoto, S., Kawasaki, M., Sulbaek Andersen, M. P., Hurley, M. D., and Wallington, T. J., "Cavity ring-down study of the visible absorption spectrum of the phenyl radical and kinetics of its reactions with Cl, Br, $Cl_2$, and $O_2$," J. Phys. Chem. A **106**, 5908–5917 (2002).
[53]Tonokura, K., Kanno, N., Yamamoto, Y., and Yamada, H., "Development of a compact laser-based single photon ionization time-of-flight mass spectrometer," Int. J. Mass Spectrom. **290**, 9–13 (2010), http://www.sciencedirect.com/science/article/pii/S1387380609003546.
[54]Tranter, R. S., Klippenstein, S. J., Harding, L. B., Giri, B. R., Yang, X., and Kiefer, J. H., "Experimental and theoretical investigation of the self-reaction of phenyl radicals," J. Phys. Chem. A **114**, 8240–8261 (2010).
[55]Trutna, W. R. and Byer, R. L., "Multiple-pass Raman gain cell," Appl. Opt. **19**, 301–312 (1980).
[56]Van Bramer, S. and Johnston, M., "Tunable, coherent vacuum ultraviolet radiation for photoionization mass spectrometry," Appl. Spectrosc. **46**, 255–261 (1992).
[57]Wang, Z., Zhang, L., and Zhang, F., "Kinetics of homoallylic/homobenzylic rearrangement reactions under combustion conditions," J. Phys. Chem. A **118**, 6741–6748 (2014).
[58]White, J. U., "Long optical paths of large aperture," J. Opt. Soc. Am. **32**, 285–288 (1942), http://www.osapublishing.org/abstract.cfm?URI=josa-32-5-285.
[59]Williams, M. W. and Arakawa, E. T., "Optical properties of crystalline $MgF_2$ from 115 nm to 400 nm," Appl. Opt. **18**, 1477–1478 (1979).
[60]Wyatt, J. R., Decorpo, J. J., McDowell, M. V., and Saalfeld, F. E., "Sampling of flow systems at atmospheric pressure," Int. J. Mass Spectrom. Ion Phys. **16**, 33–38 (1975).
[61]Xu, H. and Pratt, S. T., "Photodissociation of methyl iodide via selected vibrational levels of the $\tilde{B}$ ($^2E_{3/2}$)6s Rydberg state," J. Phys. Chem. A **119**, 7548–7558 (2015).
[62]Yu, T. and Lin, M. C., "Kinetics of the $C_6H_5$ + $O_2$ reaction at low temperatures," J. Am. Chem. Soc. **116**, 9571–9576 (1994).
[63]Zhang, F., Gu, X., Guo, Y., and Kaiser, R. I., "Reaction dynamics of phenyl radicals ($C_6H_5$) with propylene ($CH_3CHCH_2$) and its deuterated isotopologues," J. Phys. Chem. A **112**, 3284–3290 (2008).
[64]Zhang, F., Kaiser, R. I., Golan, A., Ahmed, M., and Hansen, N., "A VUV photoionization study of the combustion-relevant reaction of the phenyl radical ($C_6H_5$) with propylene ($C_3H_6$) in a high temperature chemical reactor," J. Phys. Chem. A **116**, 3541–3546 (2012).
[65]Zhou, Z., Xie, M., Wang, Z., and Qi, F., "Determination of absolute photoionization cross-sections of aromatics and aromatic derivatives," Rapid Commun. Mass Spectrom. **23**, 3994–4002 (2009).